Royal Holloway
and Bedford New College

Department of Physics

University of London

Third Year Report

Author:
Sebastian Spence
Peap011@live.rhul.ac.uk

Supervisor:
Dr. Rojas

March 31, 2021

Abstract

This report covers the bulk of work in the PhD's third year. Covering technical development of the experimental dilution fridge platform, with focus on the microwave measurement setup. Superconducting aluminium microwave cell design is also covered, with simulation of an expected g_0 for a re-entrant cell to be filled with superfluid helium. The latter part of the report covers two experimental fridge runs, one with a square aluminium cavity under vacuum and the second a re-entrant cell filled with helium.

1 Experimental Development of Fridge

This section will detail some miscellaneous additions to the fridge, made to improve it's experimental capabilities. Details for the design of experimental cells and microwave measurement circuit setup will be detailed in separate sections. This section is focussing primarily on changes made prior to the first microwave run, of elements more indirectly connected to measurement.

1.1 Silver Sinter Fill Line

The existing fridge fill lines were only present and thermalised from the room temperature (RT) plate to the heat exchanger (HX) plate. To ensure helium within the cell is thermalised to the mixing chamber (MC) base temperature, additional thermalisation in the form of a length of CuNi capillary wound around and brazed to a copper bobbin, was added at the MC stage. 0.9 mm diameter, 72% silver, 28% copper brazing wire was used, according to the recipe:

- Ramp up to 805 ℃at 7 ℃/min
- hold for 20 min
- Ramp down to 20 at 7 ℃/min with a hold back of 10 ℃

A volume of sinter was estimated from the assumption that the 0.5 mm outer diameter capillary would be tightly wound around the entire bobbin surface. This underestimated the volume by a little over 50%, as brazing the first time did not provide coverage of all the wound capillary, and a second time with 1.33× the volume of silver sinter caused the sinter to begin pooling at the bottom. So approximately 2.25× the initial estimate would be more accurate.

1.2 Hermetic Feedthrough for PreAmp Power Cable

The microwave preamp mounted inside the IVC at the 4K plate required running a DC power line down from RT. The fitted line was a 80μm copper twisted triple, installed via existing small radius tubes connecting the RT plate to the IVC, this required design of a hermetic feedthrough at RT. Due to the small opening at RT and the large connector size

of the preamp power supply cable, this feedthrough was designed in three parts (plug, housing, lid) to allow the tightening nut required for the o-ring seal over the plug part, see appendix B for drawings.

The feedthrough was designed in this way so that the twisted triple could first be epoxied into the plug, with *stycast* 1266, then passed through the housing piece and soldered to the connector attached to the lid piece. The twisted triple could then be fed down to the 4K plate, and the feedthrough attached at RT. This design has too many parts which can loosen over time, later designs were switched to prefer epoxying soldered connectors into feedthroughs. Note, using a small section of heat shrink and GE varnish at points where thin wires enters stycast, can help to prevent kinking or tearing those wires.

1.3 Minor changes

Other minor changes to the dilution fridge were made ahead of the first microwave run, these were:

- Replacement of existing legacy coaxial feedthroughs and lines to 1K. O-rings for these feedthroughs needed replacing to ensure good vacuum in the IVC and the opportunity was taken to remove these features to create more room, a better vacuum seal at RT, and reduce heat leak to 1K.
- Removal of rotating shield system for top loading to EX system. As the central hole through the fridge from RT to EX was utilised for microwave coax cables, the system to rotate plugs to cover this holes was rendered redundant (as top loading is no longer possible). Therefore this system was remove to create more space between the fridge plates and reduce heat leak between them.
- 1K pot collar. Due to the shape of the central tube through the 1K pot, used to run microwave lines, it is difficult to ensure there is no contact between lines close to their 4K thermalisation. Therefore a teflon collar has been used to provide a thermal break where a vacuum gap could not be reliably made. See appendix C for photos.

2 Cell Design

Two high purity aluminium superconducting cells were designed for this stage of the experiment. First a simple square cell was designed for characterisation of the microwave measurement circuit, and secondly a re-entrant superfluid leak tight cavity for testing the fill line, and potential measurement of g_0. For details of these types of microwave cavities please see first year report [1]. This section will discuss the evolution in design from earlier experiments and give details of how dimensions were chosen. Technical drawings of cavities can be seen in appendices D, E & F.

Both cavities use Southwest Microwave hermetic SMA pins for coupling, these pins require a specific soldering recipe described in section 3. Brass pieces were designed

for these pins to be soldered into to create a superfluid leak tight seal (as aluminium is difficult to solder). The initial feedthroughs had individual brass pieces, including a separate fill line piece, but later they were all combined into a single brass piece (subsection 2.3). Two stainless steel pieces were also designed as part of the refinement process, firstly a thin steel plate to uniformly compress the top rim of the re-entrant cavity. Then another thicker piece with threaded holes, to allow clamping of the cavity's indium seals without needing to screw into the soft aluminium.

2.1 Cell Couplings

Both re-entrant cavities and nanofludic chip cavities produce concentrated electromagnetic fields around central geometry, as discussed in previous reports [1]. This makes accurate coupling difficult as EM field strengths at open ports are low. Due to this difficulty, pin coupling was chosen over loop coupling, as fine tuning of loop: size, position, and insertion depth; cannot be achieved with accuracy, leading to a more heuristic approach [2]. Loops also often require adjustment of angle within the cavity at room temperature, not possible with nanofluidic chips as coupling is too weak above the superconducting transition. Pin couplings allow a more accurate estimation of coupling strength via tunable dimensions at the cell design stage. A more detailed treatment of both pin and loop couplings can be found in [3]. This treatment requires evaluating the field strength at microwave coupling ports which is not possible analytically for the nanofluidic cavities, however finite element modelling (FEM) with COMSOL Multiphysics can be used to simulate these cavities and estimate coupling. The simulation method was used for design of these first two aluminium cavities. Collected data can then be used to evaluate this method for later use on nanofluidic cavities. The method can be used to simplify calculations by choosing the required microwave coupling strength β:

$$\beta = \frac{Q_0}{Q_L} - 1 \tag{1}$$

Where Q_0 is the unloaded internal quality (Q) factor and Q_L is the loaded Q factor. Q_0 can be initially estimated from literature for simple cavities to $\sim 10^7$ [4], then refined with experimental data to give more accurate material properties. These simulations include the microwave ports and pin couplers, whose depth into the cavity can be tuned to give values of Q_L that correspond to a chosen β. For these experiments $\beta = 1$ (critical coupling) was chosen as this would give the strongest microwave response, and allow tuning the temperature of the experiment to move to and from critical coupling giving a more accurate determination of Q_0.

The issue encountered when calculating pin depth into the cavity is that, for centrally concentrated field, the optimal pin depth is approximately on the border of the cavity. Meaning small errors in depth can alter the pin from being slightly recessed, to being slightly into the cavity itself. These two cases represent different regimes and a significant jump in coupling. To mitigate this 45°'coupling cones' were added to the cavities, in between the microwave ports and cavity volume, creating regions of weaker field that vary slower than cavity edges. The pins can then protrude a distance into the cones, providing coupling less vulnerable to small errors in fabrication.

The method described was used to design the two microwave cavities discussed in this report, drawings can be see in appendices D, E &F. Including drawings of the redesigned lid and feedthroughs for the re-entrant cavity, discussed in subsection 2.3, the key dimensions remain the same so are not covered here (excluding cone depth reduced to $4.5mm$). The vacuum optomechanical coupling rate g_0 was also calculated from these simulations, using the method outlined in the first year report. The key parameters are:

Table 1: Comparison of key parameters for Aluminium microwave cavities.

Cavity	ω_0 GHz	Q_0 $\times 10^6$	g_0 $nHz/2\pi$	D_{cone} mm	D_{pin} mm
Square	7.37	7.63	-	3.5	0.75
Re-entrant	4.36	2.95	156	4.5	1.45

Where ω_0 is the simulated cavity microwave resonant frequency, g_0 is the vacuum optomechanical coupling rate (frequency shift of optical resonance due to the zero point motion of a mechanical resonator), D_{cone} is the depth of the coupling cone into the lid, and D_{pin} is the depth of the pin coupler into the cone. Note a lower value of Q_0 is given for the re-entrant cavity as the assumed starting Q_0 is used with the square cavity to estimate material properties for the aluminium surfaces. This assumes the dominant intrinsic loss is at the aluminium surface, therefore a higher electromagnetic field density at the surface will lead to higher losses, as in the re-entrant case.

2.2 Indium Seals

To be filled with superfluid helium a cell must be superfluid leak tight, the most common way of achieving this is via an indium seal. For the initial re-entrant cavity this meant four separate indium seals, and for the redesigned version two. 0.7 mm diameter indium wire was use for all cell seals, and two separate seal geometries were used. Both geometries assume the indium will be compressed to $\sim 50\mu m$ [5], with calculations of the distance the indium will flow being made to ensure a leak tight seal is achieved while not having flow into the screw holes or cavity itself.

Figure 1 shows both the geometries used. Firstly the diagram on the left shows the seal geometry used between the aluminium cavities lid and base. The seal if formed from by a winding an indium wire around the inside corner of the lid piece before placing it in contact with the 45°surface of the base piece. This 45°surface creates a small volume to ensure the indium does not flow too far, and that it can be compressed down to ~ 50 μm. The protrusion of the lid piece is machined to be as close to the diameter of the base piece's cavity as possible, thus creating a small as possible seam along the upper edge to reduce seam losses [6]. This small seam has the added benefit of encouraging the indium to flow into larger (estimated at 50 μm) channel away from the cavity. The pure aluminium used is very soft, so this shape of seal allows cleaning without significant deforming of the area.

Secondly the diagram on the right shows the seal geometry used between the brass pieces and the aluminium cavity lid. The design here is specifically for the SMA

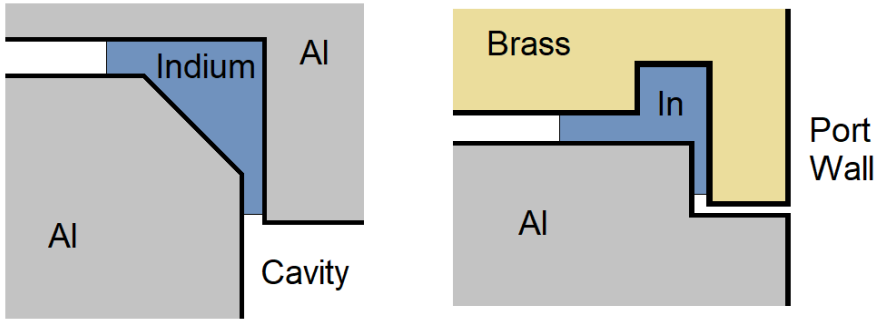

Figure 1: Figure of two indium seal methods used. Left: seal between top of aluminium cavity and base. The LHS thin section of indium is assumed to be 50 μm. Right: seal between brass pieces with SMA ports and aluminium cavity lid, shown is the LHS of an axisymmetric cross-section where the RHS is mirrored. This is the initial design, with the seal being further from the ports in the improved design but following the same principle. The LHS thin section of indium is again assumed to be 50 μm.

feedthrough pieces but has also been used for the fill line. The aim of this design is to, as closely as possible, maintain the impedance of the cavity's microwave ports. Therefore the height of the brass lip on the RHS of the diagram is such that, for 50 μm of indium thickness on the LHS, the brass surface on top of the lip (bottom on diagram) makes contact with the aluminium surface opposite. This minimises the jump in impedance mismatch of the line, reducing reflection from the feature. Similarly to above there is a volume for the indium to be compressed into, reducing the flow distance and giving a more reliable compression to 50 μm. The seam on the RHS bottom of the volume is also kept small to encourage the indium to flow to the LHS, reducing the risk of it flowing onto the lip and preventing contact.

2.3 Re-entrant Redesign

Appendix E shows the initial design of the re-entrant cavity pieces, while appendix F shows the redesigned pieces. The brass pieces were redesigned into a single additional brass lid piece, this meant a new aluminium cavity lid also needed to be designed, and due to drilling out of the threaded base holes another steel clamp with threaded screw holes was designed. The main reason for these redesigns were problems arising from the softness of pure aluminium, though this chance was taken to make other improvements. Initially a stainless steel collar was designed (figure 25) to clamp the thin outer ring of the cavity lid, which would deform between the outer screws. This worked for distributing the pressure around the cavity's indium seal, however it did not help the softness of the threaded aluminium. It was not possible to reliably apply sufficient torque to screw threads for leak-tight seals, before tearing the aluminium screw threads. An attempted fix was made with helicoils, however these proved insufficient and the entire thread would tear.

It was decided to redesign the three individual brass pieces attaching to the aluminium lid, into a single large brass disc piece that would act like an additional lid (figure 27. Thus removing all screws other than the larger M3 screws through the outside wall of the cavity. The threaded M3 screw holes on the outside of the aluminium base piece were then drilled into through holes. In order to clamp the cavity, another stainless steel piece was designed with threaded M3 holes 28, allowing the cavity to be tightened between the two steel pieces, removing any need to screw directly into aluminium from the design. The new brass piece required a new aluminium lid piece with appropriate indium seal (figure 26), so a nub was added to the brass corresponding to a socket in the new lid, to ensure good alignment of the coupling pins.

The redesign had the advantage of reducing the total number of indium seal from four to two, and moving the indium seals to the outside of the cavity. With only the two SMA feedthroughs as additional possible sources of leaks, this made identifying leaks much simpler. The initial brass feedthrough pieces were difficult to remove without accidentally bending the coupling pins against the aluminium ports, which also damaged the aluminium. This risk is reduced on the redesign as the brass lid's indium seal can be broken via the brass M3 threads. Figure 2 shows the cavity when fitted to the EX stage of the fridge.

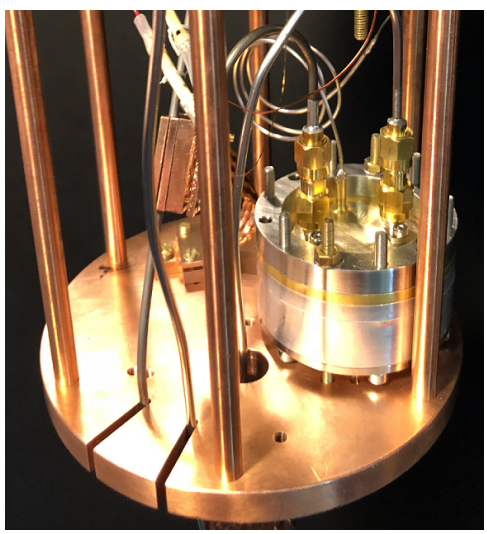

Figure 2: Picture of experimental stage of dilution fridge, showing fully installed re-entrant cavity, post redesign. With both microwave lines and fill line attached. Microwave lines run from MC above to below the EX stage where the final attenuator is on the down line, and the circulator is for the return. The cell is bolted together with six stainless steel screws, then held to the EX stage with two brass screws.

The modified cavity has screws protruding below, so the aluminium no longer makes direct contact with the EX stage, to ensure thermalisation a copper disc has been added between the bottom of the cavity and the EX stage. New cavities going forward will take into account the new clamping method and recess the screws. Another improvement would be thinning the fill line extension from the brass pieces, as this was too thick to easily solder. It may also be possible to only use one steel clamping piece, having the

threaded steel clamp on the bottom and clamping with the brass on top, though available screw size will need to be taken into account.

3 Hermetic Feed-through Solder Recipe

To achieve superfluid leak tight microwave feethroughs, soldered in glass bead hermetic seals from *Southwest Microwave* were used. Figure 27 shows the redesigned brass lid with the pilot holes for these seals. Appendix G then shows the installation procedure and the dimensions of the hole required for soldering. *290-02G* glass bead seals were used, in holes drilled by specialised drill piece *T-291-4*. The pins were connected to using *214-522SF* super SMA jacks which are mounted by small screws either side, which are also used by the solder tool *T-212-5*, having similar form to the SMA jack.

Once the correct hole profiles are drilled the beads must be soldered in place. This process is designed for non-accessible specific solder split rings, so to achieve a hermetic seal while maintaining a good impedance match requires careful handling. The current process used in the lab is:

- Heat copper piece with holes on hot plate to 100℃(the copper piece with holes is to allow the coupling pins to stick down without the base of the hot plate pushed the beads out)
- Apply acid flux to brass drilled hole
- Place brass piece on top of the copper and allow the flux to fully melt
- Remove the brass piece, clean with IPA and allow to cool
- Heat hot plate and copper to 300℃
- Place brass piece onto another room temperature copper piece with holes such that beads can be fully inserted (long pin down).
- With the bead in place create a solder wire split ring by wrapping around the insert part of the solder tool and cutting.
- With solder tool place this ring over bead and use a wooden stick to push it into the groove around the bead.
- Repeat this process until three rings have been pushed into the groove, flux can be applied lightly to the rings.
- The solder tool can be screwed on to push the last split ring into place.
- Once the last ring is in place use a cotton bud to remove any excess flux.
- Tighten the solder tool onto the piece and place onto the hot plate.
- Leave for ∼5 mins or until the solder tool is hot enough to melt solder on contact.

- Remove the piece from the hot plate and cool by dipping edge in water (not getting the feedthrough area wet).
- Remove the solder tool when cool and clean with IPA.
- Gaps in the solder join can be filled by placing a small amount of solder and flux into the area and placing back on the hot plate.
- Excess solder spilling out onto the brass can be carefully filled away without affecting the impedance matching, provided the outer metal of the bead is not damaged.

This method has proved effective at forming superfluid leak tight seals, tested up to 2 bar, with acceptable impedance matching. 0.23 mm diameter tin-silver solder is used with a melting point of 217 ℃, 300 ℃is used as the solder must be heated through the copper and brass pieces. The solder wire must be this thin to fit into the groove around the bead, however solder this thin sold commercially is only flux core tin-silver, which may not be the best for this application. It is difficult to not have gaps in the solder around the bead after heating, these gaps may only be on the surface and the connection may still be leak tight but this is still concerning. This could be caused by insufficient solder inside the groove, too much flux, the wrong solder type, or insufficient heating. An alternative is to use more standard flux free tin-lead solder that has been rolled/compressed into a thin enough shape to fit into the gap, this could allow tighter control of the amount of solder used, and the solder type may flow better inside the gap. This soldering can also be performed inside a helium / nitrogen environment when soldering into copper to prevent oxidation.

4 Microwave Measurement Circuit

For microwave measurement a two line (in/out) microwave measurement circuit was installed on the dilution fridge. This section will give details of the set-up and discuss some basics of the measurement.

4.1 Circuit Design

The mounted circuit follows a fairly simple design for microwave measurement down to mK temperatures, using an attenuated 'in' line to bring signal down to the device under test (DUT), then an amplified low attenuation 'out' line to return the signal modified by the DUT to a detector. Figure 3 shows a diagram of this measurement setup, including all microwave components and thermalisation at each plate. The in line is attenuated at each plate (except the still) to reduce the heating power applied to the lower plates and DUT. The attenuators have the effect of thermalising the cable core at each plate while reducing the signal intensity and radiation noise. As attenuation is required on the in line, cables can be chosen to minimise thermal conductivity without too much concern for their attenuation. For the out line reducing signal losses is the priority, therefore superconducting coax is used up to 4K and then lower loss coax to

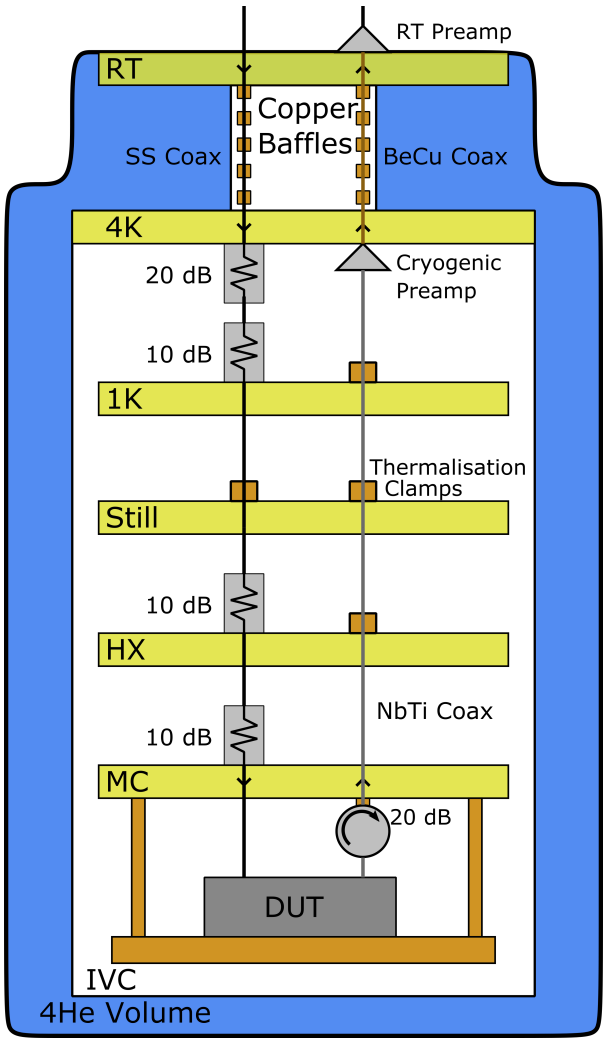

Figure 3: Figure showing microwave circuit inside the dilution fridge.

RT. The relatively low power signal exiting the DUT is also amplified, before coming into contact with higher temperature components to improve its signal to noise ratio, allowing better measurement sensitivity. The line is amplified by both a cryogenic preamp at 4K (itlLNF-LNC0.3 14A s/n 1628Z), and a preamp at RT (*LNF-LNR1 15A*). These amplifiers generate noise that can easily travel back down the low attenuation out line and into the DUT disturbing the measurement, this is negated by a $20dB$ isolator (itlLNF-ISC4-12A s/n 1901-15) mounted on the EX plate. All three components are from low-noise factor.

Table 2: Comparison of coaxial cables used in microwave circuit. Both attenuations given for 5 GHz signal.

Inner Material	*Outer Material*	*Thermal Conductivity @4K(Wcm/K)*	*Attenuation @300K(dB/m)*	*Attenuation @4K(dB/m)*
Ag Plate BeCu	BeCu	4.88E-04	1.8	0.6
SUS304	SUS304	4.30E-05	9.4	5.9
NbTi	NbTi	2.64E-05	9.6	<0.3

The properties of the coaxial cables used for the in and out lines are shown in Table 2 below. All coax are *Coax CO., LTD* semi-rigid cables with SMA male connectors, of part number *SC-219/50-Core Mat-Outer Mat-Length-SMAP/SMAP* (eg. SC-219/50-SS-SS-1400-SMAP/SMAP for full stainless steel 1400 mm). All coaxial cables for the in line are stainless steel SUS304 with lengths: 1400 mm RT-4K, 300 mm 4K-1K, 300 mm 1K-HX, 400 mm HX-EX and 400 mm EX-DUT. While on the out line the 4K-RT cable is 1400 mm BeCu, then NbTi 1000 mm EX-4K and 300 mm DUT-EX.

These lengths become important when calculating the noise delivered to the DUT by the in microwave line at the operating frequency ($\sim$5 GHz). The noise photon occupation number $n_i(\omega)$ at stage i and frequency ω can be calculated according to[7]:

$$n_i(\omega) = \frac{n_{i-1}(\omega)}{A_i} + \frac{A_i - 1}{A_i} n_{BE}(T_{i,att}, \omega) \tag{2}$$

Where $n_{i-1}(\omega)$ is the noise photon occupation number at the previous fridge stage (plate), A_i is the attenuation at the ith plate, and $n_{BE}(T_{i,att}, \omega)$ is the Bose-Einstein distribution at the temperature of the ith plate's attenuator. This formula allows calculation of the noise photon occupation for each plate in turn down to the DUT itself. This formula does not explicitly take into account the resistance of the coaxial cables themselves, however this can be estimated by assuming the half of the coax closest to each plate is at that plates temperature. From here it is a simple matter of calculating $n_i(\omega)$ at each plate, starting with $n_{RT}(\omega) = n_{BE}(300K, \omega)$. At 5 GHz this gives $n_{DUT} = 0.023$ for our experimental setup. This is closer to the occupation level needed for a qubit experiment and so may be overkill for what we require, however running with this level of isolation will be a good test of the circuit's overall sensitivity.

4.2 Mounting Design

Due to the age of the dilution fridge it is not designed for modern microwave measurement setups, therefore care was taken to design mounting that would both fit the space and thermalise the measurement circuit. From RT to 4K both the in and out lines run through a central tube, these cables are mounted to a set of copper baffles with skirts that should provide thermal contact with the inside of the tube, thermalising the cable on the way down while blocking thermal radiation from RT. From 4K down most components are thermalised in a 'floating' scheme, where components are thermalised to one end of copper (or gold plated copper) braids, which are then thermalised at the other end to the fridge plates. There are two main types of these thermalisation clamps, one that clamps all the attenuators (Figure 4), and the other that clamps the coaxial line itself (Figure 5). The cryogenic preamp is also thermalised via a floating braid. These braids

are used where the space provided is not sufficient for direct mounting according to the minimum bend radii of the coaxial cables.

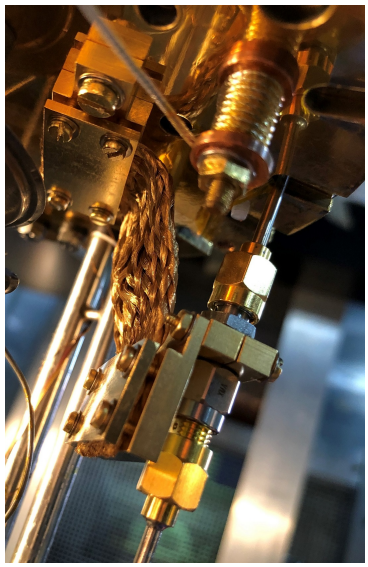

Figure 4: Figure showing the floating braid thermalisation for attenuators.

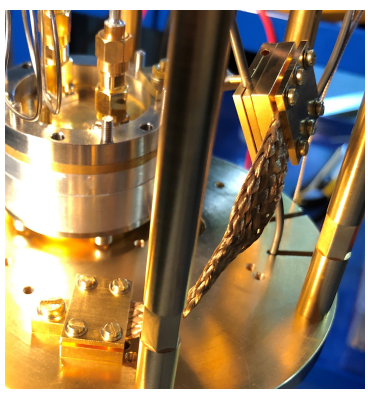

Figure 5: Figure showing the floating braid thermalisation for coaxial cables themselves.

Towards the MC thermalisation becomes increasingly important, especially thermalisation of EX stage components to the MC base temperature. Therefore the copper components from HX down are gold plated to increase thermal contact and stop the copper surfaces from oxidising. The microwave cells (DUT) are thermalised by clamping directly to the EX plate, and the circulator directly to a pillar on the bottom of the EX plate. The EX plate itself is then clamped to the MC plate via six gold plated copper rods, ensuring it is well thermalised to base temperature.

4.3 S_{21} Derivation

Initial measurements take the form of S_{21} transmission measurements on the fridge circuit shown in Figure 3. A treatment of the circuit response is required to analyse the data

from these measurements. Generally the circuit is treated as a flat level around the cavity resonance, the sum total of attenuation and amplification, including a noise floor term and also an overall circuit phase. This assumption is based upon the narrow resonance expected from the superconducting microwave cavity, with the rest of the circuit response assumed to be constant over such a narrow bandwidth.

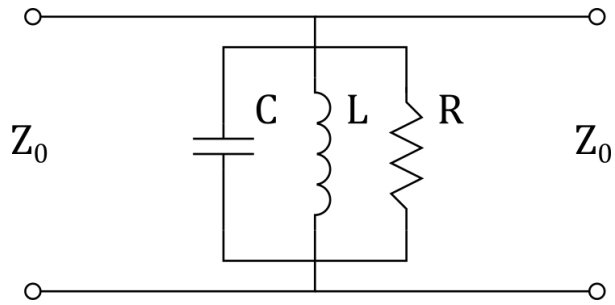

Figure 6: Figure showing parallel RLC representation of microwave circuit, set in a two port network with port impedances Z_0.

Microwave cavities can be abstracted to lumped element RLC circuits, in this case a parallel RLC circuit as show in Figure 6. This RLC circuit will have the characteristic impedance:

$$Z(\omega) = \left(\frac{1}{R} + i\omega C + \frac{1}{i\omega L}\right)^{-1} \tag{3}$$

Where ω is the angular frequency of the signal incident on the circuit, R is the characteristic resistance, C the capacitance, and L the inductance. This circuit describes a cavity with resonant frequency $\omega_0 = 1/\sqrt{LC}$ and quality factor $Q = \omega_0 RC = R/\omega_0 L$. Using the substitution $\Delta\omega = \omega - \omega_0$ and the approximation:

$$\omega^2 - \omega_0^2 \approx 2\omega(\omega - \omega_0) \tag{4}$$

Near to ω_0 allows simplification of the impedance into the form:

$$Z = \frac{R}{1 + 2iQ\delta\omega} \tag{5}$$

Where the additional substitution $\delta\omega = \Delta\omega/\omega_0$ has been made. Switching to admittance $Y = Z^{-1}$ gives:

$$Y = \frac{1}{R} + \frac{2iQ\delta\omega}{R} \tag{6}$$

Then using the general ABCD transmission matrix for a general admittance in parallel [8]:

$$\begin{bmatrix} A & B \\ C & D \end{bmatrix} = \begin{bmatrix} 1 & 0 \\ Y & 1 \end{bmatrix} \tag{7}$$

With the general S_{21} for a two port transmission measurement of admittance Y with characteristic port impedances Z_0 (Figure 6):

$$S_{21} = \frac{2}{A + B/Z_0 + CZ_0 + 1} \tag{8}$$

Gives an expression for the transmission:

$$S_{21} = \frac{\beta}{(\beta + 1) + 2iQ_0\delta\omega} \tag{9}$$

Where $Q = Q_0$ from above and the substitution $\beta = 2R/Z_0$ has been made. This β is the coupling constant of the microwave system, representing the ratio of the internal and external quality factors $\beta = Q_0/Q_e$, with $Q_e = z_0/2\omega_0 L$ coming from the definition of an RLC terminated on two ports with Z_0 impedances. Here the internal quality factor Q_0 represents energy dissipated within the cavity itself, while the external quality factor Q_e represents energy drawn out of the cavity through couplings, including the energy terminated in a measurement device. The total quality factor of the combined system is $Q_L = (Q_0^{-1} + Q_e^{-1})^{-1}$, know as the loaded Q.

However with this simple circuit directly coupling the RLC resonator to a measurement, the high Q_0 resonance will be destroyed by a low Q_e, due to $R \gg Z_0$. This, along with the impracticality of coupling directly to a cavity mode, means some coupling scheme must be employed to mediate the flow of energy out of the resonator. The two usual methods are loop couplers which couple to the magnetic field of the cavity, or pin couplers which couple capacitively to the electric field [3]. Pin couplers are used here, one port represented by C_e in Figure 7, the other port can be mirrored on the RHS.

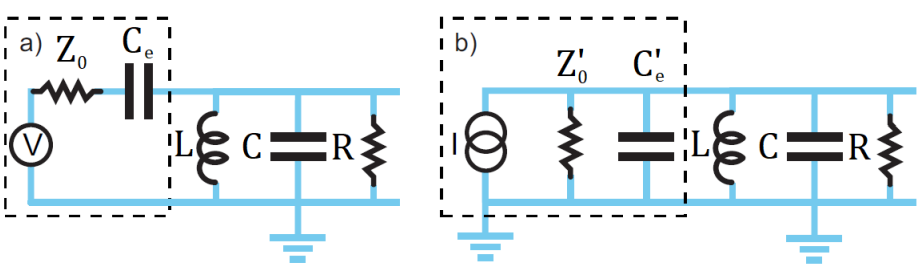

Figure 7: Figure showing the Thevenin-Norton source transformation for capacitive coupling to an RLC resonator.

It is possible to use reformat the capacitively coupled circuit into a form where Equation 9 can be used. This involves using the Thevenin-Norton source transformations[9], along with basic admittance and impedance transforms. A visualisation of the process is shown in Figure 7, where there are equivalent parallel lumped elements to the more physical series ones. This shows the transform for one port, but the process can be mirrored on the RHS for the second port.

The series components represent an impedance of:

$$Z_1 = Z_0 + \frac{1}{i\omega C_e} \tag{10}$$

While the parallel components represent an impedance of:

$$Z_2 = \left(\frac{1}{Z_0'} + i\omega C_e'\right)^{-1} \tag{11}$$

The equivalence is that there exists Z_0', C_e' such that $Z_1 = Z_2$. This is also true for admittance and simpler in this form. The equivalent parallel admittances are:

$$Y_1 = \left(Z_0 + \frac{1}{i\omega C_e}\right)^{-1} \tag{12}$$

$$Y_2 = \frac{1}{Z_0'} + i\omega C_e' \tag{13}$$

Y_1 can be expanded and simplified into the form:

$$Y_1 = \frac{q^2/Z_0 + i\omega C_e}{1 + q^2} \tag{14}$$

Where $q = Z_0 \omega C_e$ can be thought of as the charge on the coupling capacitors[9]. For a weak coupling $q \ll 1$ $(1 + q^2 \approx 1)$, Y_1 can be approximated to:

$$Y_1 = \frac{q^2}{Z_0} + i\omega C_e \tag{15}$$

Comparing this form of Y_1 to Y_2 it is clear that $Z_0' = Z_0/q^2$ and $C_e' = C_e$. The parallel capacitance C_e' can then be taken into the cavity capacitance C, while Z_0' becomes the new characteristic impedance of the transmission circuit. This leads to an equation for S_{21} of the same form as Equation 9, with the modifications $\beta \Rightarrow 2Rq^2/Z_0$ and $C \Rightarrow C + 2C_e$ (mirroring for a second port). The equation for S_{21} can also be written as:

$$S_{21} = \frac{Q_L/Q_e}{1 + 2iQ_L\delta\omega'} \tag{16}$$

Where $Q_e = Z_0/2q^2\omega_0' L$ and $\delta\omega' = (\omega - \omega_0')/\omega_0'$, using $\omega_0'^2 = 1/L(C + 2C_e)$ as the modified resonant frequency of the cavity. The capacitance of the coupling is expected to be small compared to the cavity capacitance, therefore the modification to ω_0 can be largely ignored (or modelled for with FEM). Taking into account a general microwave circuit response outside of the cavity gives:

$$\widetilde{S_{21}} = A + Be^{i\phi}\frac{Q_L/Q_e}{1 + 2iQ_L\delta\omega'} \tag{17}$$

Where A is a complex number number representing the floor of the experiment with an arbitrary phase, B represents the total attenuation and amplification of the circuit, and $e^{i\phi}$ is the phase shift of the circuit. As the Q is so high these experimental factors are assumed to be constant over the region of interest. From a single experimental measurement it is not possible to determine Q_0 or Q_e, due to the arbitrary B factor, however in a very over-coupled regime Q_L will be dominated by Q_e and in a very under-coupled regime Q_0 will dominate. It may also be possible to determine these separate Q's across multiple measurements at varying temperatures.

Note in [9] the approximation for q is given only for 'weak' coupling, however with the coupled circuit:

$$q^2 = \frac{Z_0\beta}{2R} \tag{18}$$

This is almost always very small. $Z_0 = 50\Omega$ and $R \approx 1 \times 10^{12}\Omega$, while β can vary a few order of magnitude around 1, it is unlikely the approximation $q^2 + 1 \approx 1$ is never not valid. The 'weak' coupling here then refers to an absolute weak coupling, meaning a high Q_e in absolute terms rather than it's relationship to Q_0. Additionally q is dependent on ω but this variation is assumed to be small over the region of interest.

4.4 Maximum Power

The VNA used to measure S21 through the fridge circuit has a max output power of 0 dBm in the region of interest (300 kHz to 8.5 GHz), and a max input power of 6 dBm (>26 dBm will damage the instrument). The in line to DUT has ∼70 dB of attenuation while the return line has ∼20 dB of amplification without the RT preamp, so it will not be possible to overload the VNA without additional amplification. In practise, when amplifying the input signal, the heat delivered to the MC will become too large before the 6 dBm max at the VNA input is reached. The attenuation before the MC is ∼55 dB, assuming all power past this is delivered to the MC then the signal at the MC should be kept below -10 dBm (∼100 μW), meaning a power delivered to the top of the fridge of at most 45 dBm. Though care should be taken when including amplification before and after the fridge to ensure power stays below the VNA max.

5 Square Cell Run

5.1 Experimental Details

The fridge was successfully run down to a minimum base temperature of 27.2 mK, and measurements made of the square superconducting microwave cavity. Each run of the fridge allows for a refinement of the cooling down and warming up process, this refinement is used to update the created fridge manual [10]. The changes between this run of the fridge and the last have been covered in detail, including minor changes in Section 1.3. One difficulty discovered was that microwave measurements are not possible above the superconducting transition of the aluminium, this is due to the high attenuation on the line in and the low quality factor of the cavity below this transition.

5.2 Results

Shown in Figures 8 and 9 is some of the best VNA measurement data of the square cavity at a base temperature of ∼28 mK. The data has been fitted to $\tilde{S}_{21}$ from Equation 17, giving a ω_0 of 7.60 GHz and Q_L of 1.78×10^5. As discussed previously it is not possible to extract the internal quality factor from this measurement alone. It would be

difficult to accurately extract this from measurements over a range of temperatures for this system, as it is very over-coupled (inferred via the decreasing peak amplitude with decreasing temperature). For the next generation of superconducting microwave cavities, increasing the estimated internal quality factor when calculating the pin depth for critical coupling should allow more direct measurement of Q_0, alternatively an under-coupled system could be designed where Q_0 is dominant.

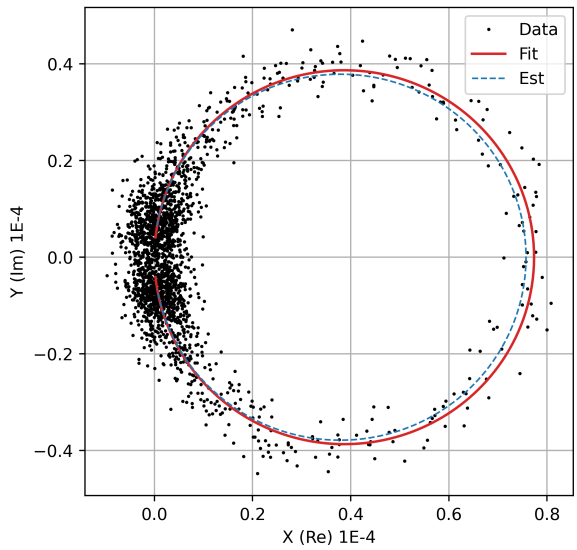

Figure 8: Figure showing circle plot $S_{21}(\omega)$, for square cavity. The plot has been re-centred but not normalised in magnitude. X is the real part of $S_{21}(\omega)$ and Y is imaginary. VNA re-centred data is represented by black dots, the initial fitting estimate by the blue dashed line and the full fit by the solid red one.

5.3 NbTi Coax Issue

During this run there was a sporadic issue with $S_{21}(\omega)$ measurements of the cavity resonance at base temperature. Sometimes the resonance peak (in magnitude) would cut-off some distance towards the peak, into either: a flat top, another peak shifted down a few dB, back to the noise floor or a flat level above the noise floor. The higher frequency tail of this peak would be recovered for all but the cut-off back to the noise floor. This would occur when the helium bath was fairly low and when the VNA signal was amplified beyond a certain point, with the lower the bath got the lower the input power threshold before this behaviour occurred. It is believed that this issue is caused by the 4K plate rising in temperature as the bath level drops. This could lead to the NbTi superconducting coaxial cable at the cryogenic preamp being closer to it's superconducting transition temperature (with extra heating from the preamp itself). Then as the VNA sweeps closer to the resonance the power through the cavity could increase to a point where it heats the NbTi near the preamp, which causes a compounding effect where more of the cable goes normal, causing more heating etc.

Two methods were employed to try and mitigate this effect. Firstly a copper braid

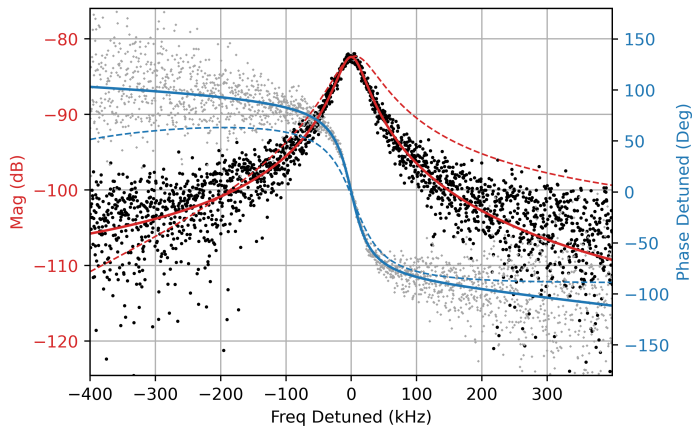

Figure 9: Figure showing LogMag and Phase of $S_{21}(\omega)$, for square cavity. The plot has been re-centred but not normalised in magnitude. The plot is in detuned frequency from resonance, plotted against magnitude in dB and phase in degrees. VNA re-centred data is represented by black dots for magnitude and grey for phase, red lines correspond to fits of magnitude and blue for phase, the initial fitting estimate by the dashed lines and the full fit by the solid ones.

was attached to the top of the 4K plate, running outside the IVC and down into the bath volume, this should help the 4K plate to remain closer to 4K. Secondly a small heat leak was created using a copper wire from the 1K pot to the small section of copper coax between the preamp and NbTi cable, this should provide additionally cooling after the thermalisation to 4K to ensure the NbTi remains below its superconducting transition temperature. The heat leak was estimated to be around 1 mW, from it's length and RRR.

6 Re-entrant Run

6.1 Experimental Details

As discussed earlier the silver sintered fill line thermalisation to the MC was added before this run, the fill line used is labelled Y. Pi filters (*51F-744-002, 5500pF*) were also added at the MC before the MC thermometer, to reduce the heating of this thermometer due to AC noise in the line. Silver tape was also added to the helium bath baffles to plug holes and hopefully increase the cooling efficiency to 4K of the fridge. The minimum base temperature for this run was 24.9 mK, suggesting an improvement likely due to the addition of pi filters.

This run was for the superfluid leak tight re-entrant cavity discussed above, making use of the fill line from RT and the fill line gas handling system outside the fridge. The cell was filled with helium to around 1 bar, but there was only time for VNA measurements to be taken. The run had to be aborted for two reasons: firstly the lab was closing down due to the pandemic, and secondly the gas handling system had significant leaks. Closing the filled cell at the top of the fridge would stop any leak affecting measurement, but leaving the cell full and closed could present a hazard if the fridge were to warm up

unsupervised. While leaving the cell open to the gas handling system could mean air freezing into the fill line, which also presents a hazard. This could be partially mitigated by a cold trap, but the current trap does not stay cold overnight.

6.2 Results

Table 3: Comparison of cavity resonances and quality factors.

Temperature	*Fill*	$\omega_0/2\pi$ GHz	Q_L
300 K	Vacuum	4.28	3.54×10^3
4 K	Vacuum	4.31	1.76×10^4
27 mK	Vacuum	4.31	1.46×10^5
25 mK	^{4}He	4.19	1.55×10^5

Table 3 shows data collected on this run. For room temperature the VNA is connected directly to the cavity under vacuum, as measurement through the fridge microwave circuit is not possible. Figure 10 show data for this room temperature experiment, while Figures 11 and 12 show data for 4 K and 25 mK respectively. Visually the data of the cavity filled with helium looks very similar to under vacuum, other than a shift in resonance frequency. Experimental factors lead to small fluctuations in Q_L and ω_0, and while the helium produces a noticeable shift in ω_0 it does not with Q_L, this is as expected as helium's dielectric loss should not be the limiting factor here.

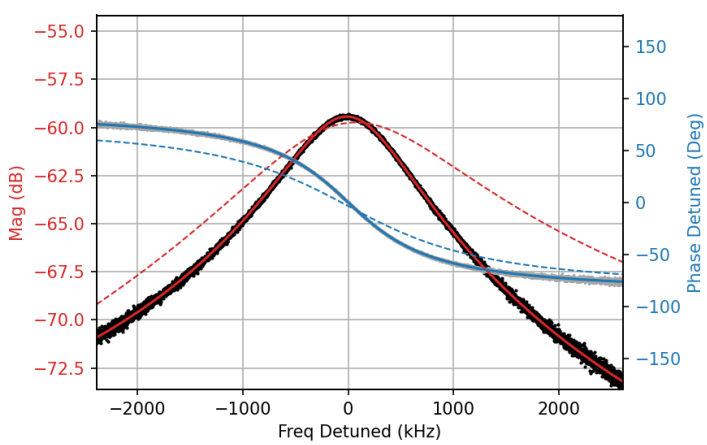

Figure 10: Figure showing LogMag and Phase of $S_{21}(\omega)$, for Re-entrant cavity at RT. The plot is in detuned frequency vs logmag and phase. VNA data is represented by black dots for magnitude and grey for phase, red lines correspond to fits of magnitude and blue for phase, initial fitting estimates by dashed lines and full fit by solid ones.

This run also suffered the cavity being very over-coupled to the measurement setup, this can be seen from the small single order of magnitude increase in Q_L going below the aluminium's superconducting transition temperature. Such a small increase in Q_L

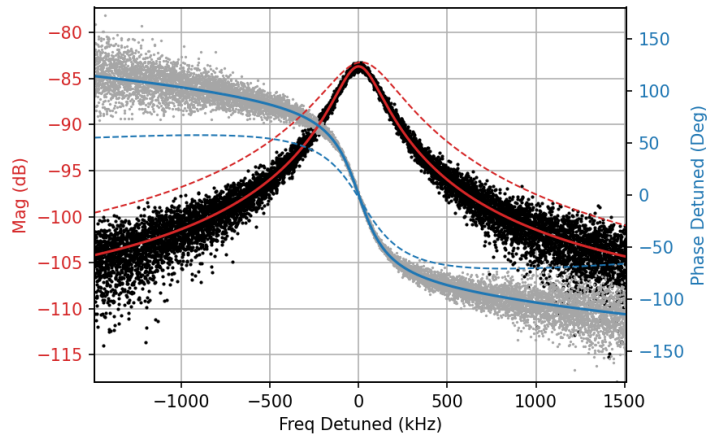

Figure 11: Figure showing LogMag and Phase of $S_{21}(\omega)$, for Re-entrant cavity at 4 K. The plot is in detuned frequency vs logmag and phase. VNA data is represented by black dots for magnitude and grey for phase, red lines correspond to fits of magnitude and blue for phase, initial fitting estimates by dashed lines and full fit by solid ones.

suggests we are limited by Q_e, though less so than the square cavity as it is possible to see the resonance at 4 K, likely due to the concentration of the electric field above the stub making weaker coupling much easier. It may be possible to find the internal quality factor by looking at how the S_{21} measurements vary with temperature, though it is likely the system is so over-coupled this will be difficult. The internal Q may also be found via the external Q, by varying temperature until critical coupling (a maximum of peak height), where the internal and external Q's should be equal. Then is is a matter of setting this external Q for lower temperatures to extra internal, relying upon the external Q not varying significantly with temperature.

Measurement of g_0 was not possible for this run, firstly because there was no mechanical drive (e.g. a piezo fitted to the outside of the cavity), and secondly because there was no time for a more careful search using optomechanical motion. It is also likely that applying a drive tone via the microwave in line would apply too much heat to the MC, if this becomes necessary it would be possible to reduce the attenuation at the lower stages, to measure something more classically driven.

Other modes were visible at higher frequencies, in fairly good alignment ($\sim$10%) with COMSOL estimated resonant frequencies, however we are focussing on the fundamental mode as it should couple more strongly to the mechanics of the system.

7 Future Plans

In terms of the fridge experiments a piezo will be added before the next run to drive the helium acoustic modes, and a reliable higher pressure gas handling system will be constructed. This should allow a full optomechanical experiment with the re-entrant cavity, hopefully including optomechanically induced transparency and thermomechanical motion measurements.

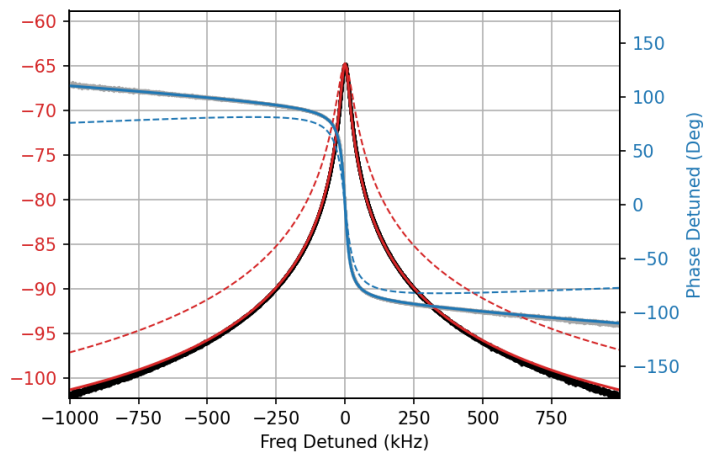

Figure 12: Figure showing LogMag and Phase of $S_{21}(\omega)$, for Re-entrant cavity at 25 mK. The plot is in detuned frequency vs logmag and phase. VNA data is represented by black dots for magnitude and grey for phase, red lines correspond to fits of magnitude and blue for phase, initial fitting estimates by dashed lines and full fit by solid ones.

During the first lockdown we have also been working on a simulation and theory paper for the nanofluific sonic crystal chip proposal, in prepublication [11]. This will be a useful part of my thesis.

We have also been working on a room temperature experiment with SiN membranes inside re-entrant cavities, looking for thermomechanical motion. Developing this experiment towards a publication will also be useful for developing microwave measurement theory and experimental skills.

The nanofabrication of our nanofluidic chips needs to be carried out, cleanroom access has been prevented for a large part of the pandemic. However cleanrooms are opening up now, so it may be possible to use either LCN or SuperFab (at Rhul), another option if this does not seem practical is to contract this out privately.

There is also the possibility of a SiN membrane experiment at low temperature, which would be similar enough to the room temperature experiment to be quick to implement. A more developed version of this would be an on chip re-entrant cavity, either with a membrane or filled with helium, though this may be beyond the scope of the PhD in terms of time.

References

[1] S. Spence, "First year report," tech. rep., Royal Holloway University, 2020, peap011@live.rhul.ac.uk.

[2] L. A. De Lorenzo, *Optomechanics with superfluid helium-4*. PhD thesis, California Institute of Technology, 2016.

[3] M. J. Reagor, *Superconducting cavities for circuit quantum electrodynamics*. Yale University, 2016.

[4] M. Reagor, H. Paik, G. Catelani, L. Sun, C. Axline, E. Holland, I. M. Pop, N. A. Masluk, T. Brecht, L. Frunzio, *et al.*, "Reaching 10 ms single photon lifetimes for superconducting aluminum cavities," *Applied Physics Letters*, vol. 102, no. 19, p. 192604, 2013.

[5] C. Lim, "Indium seals for low-temperature and moderate-pressure applications," *Review of scientific instruments*, vol. 57, no. 1, pp. 108–114, 1986.

[6] T. L. Brecht, *Micromachined quantum circuits*. PhD thesis, Yale University, 2017.

[7] S. Krinner, S. Storz, P. Kurpiers, P. Magnard, J. Heinsoo, R. Keller, J. Luetolf, C. Eichler, and A. Wallraff, "Engineering cryogenic setups for 100-qubit scale superconducting circuit systems," *EPJ Quantum Technology*, vol. 6, no. 1, p. 2, 2019.

[8] D. M. Pozar, *Microwave engineering*. John Wiley & Sons, 2009.

[9] D. I. Schuster, *Circuit quantum electrodynamics*. Yale University, 2007.

[10] S. Spence, "Fridge manual: Screen room w061 dilution fridge operation," tech. rep., Royal Holloway, 2020, peap011@live.rhul.ac.uk.

[11] S. Spence, Z. Koong, S. Horsley, and X. Rojas, "Superfluid optomechanics with phononic nanostructures," *arXiv preprint arXiv:2012.10816*, 2020.

Appendices

A Copper Anneal Recipe

Below is a copper annealing recipe previously used to increase the conductivity of a copper re-entrant cell. However this decreased the overall microwave quality factor so has not been repeated for later copper cells, this is likely due to surface effects. The recipe used was:

- 950 ℃in vacuum for 9+ hours (we did 12)
- 850 ℃for ∼12 hours in dry air
- passing a small amount of air across the piece to the pump, pressure should be 10^{-4} $mbar$ at the cavity.

B Preamp Feedthrough Drawings

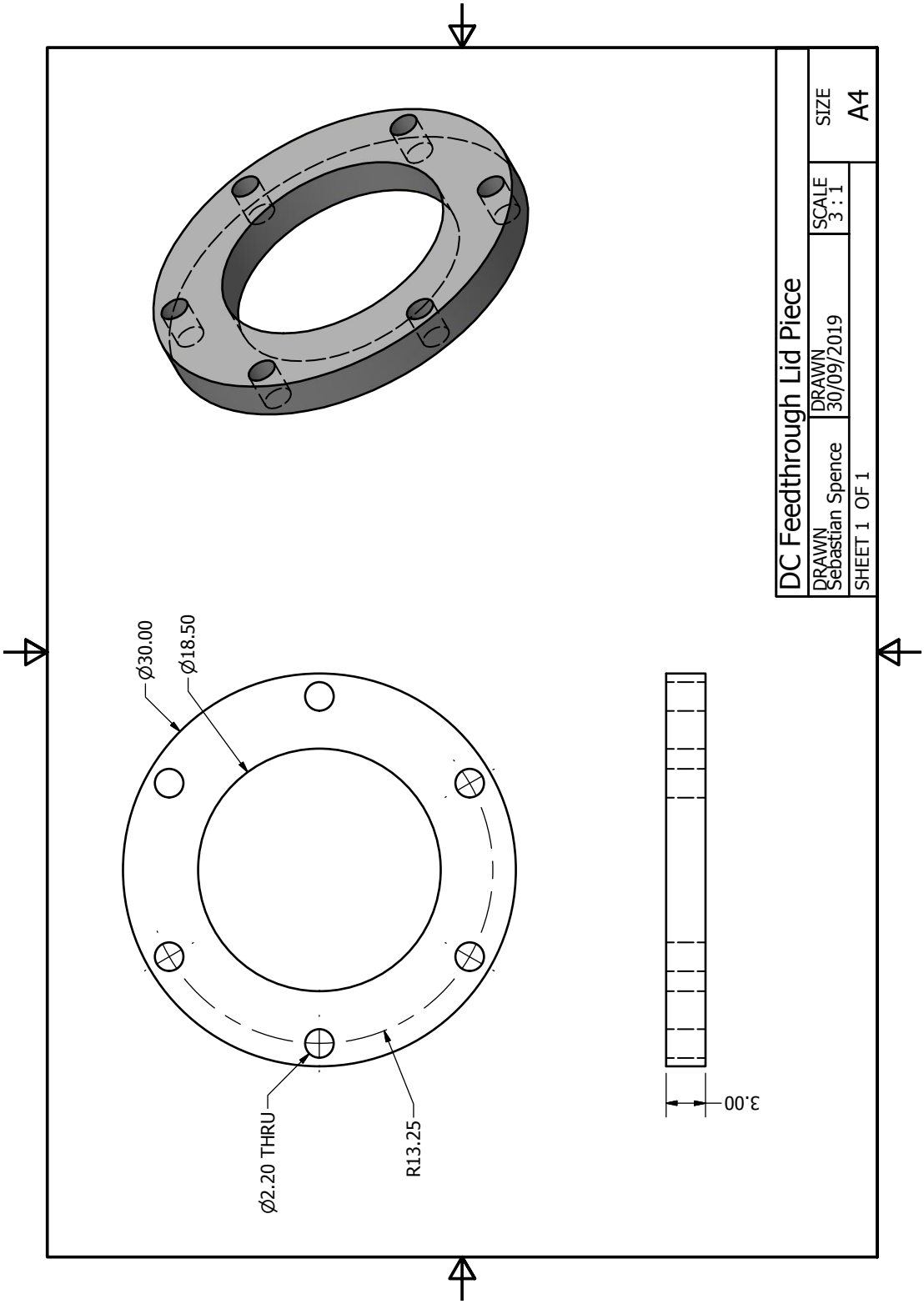

Figure 13: Lid piece for preamp feedthrough.

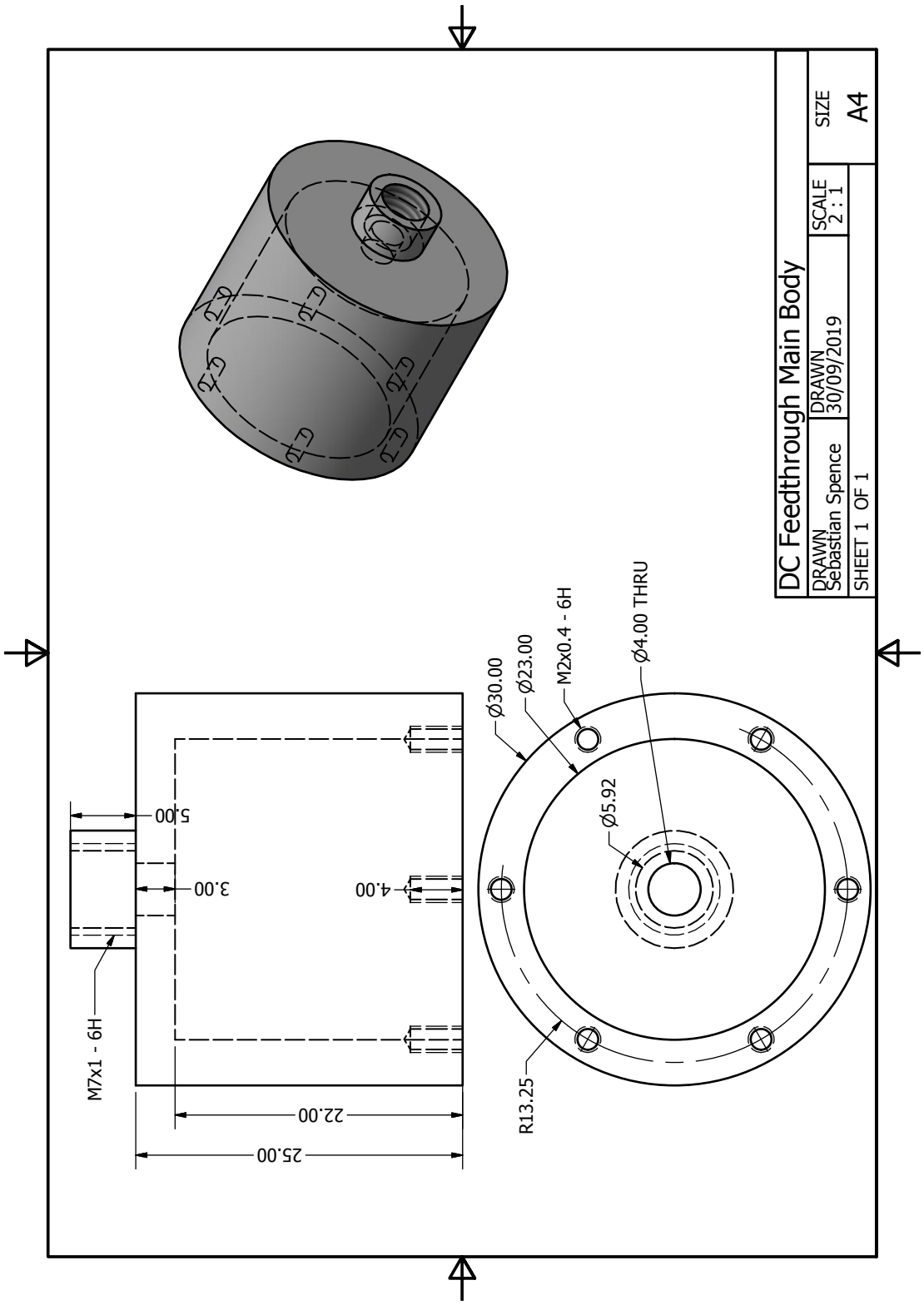

Figure 14: Housing piece for preamp feedthrough.

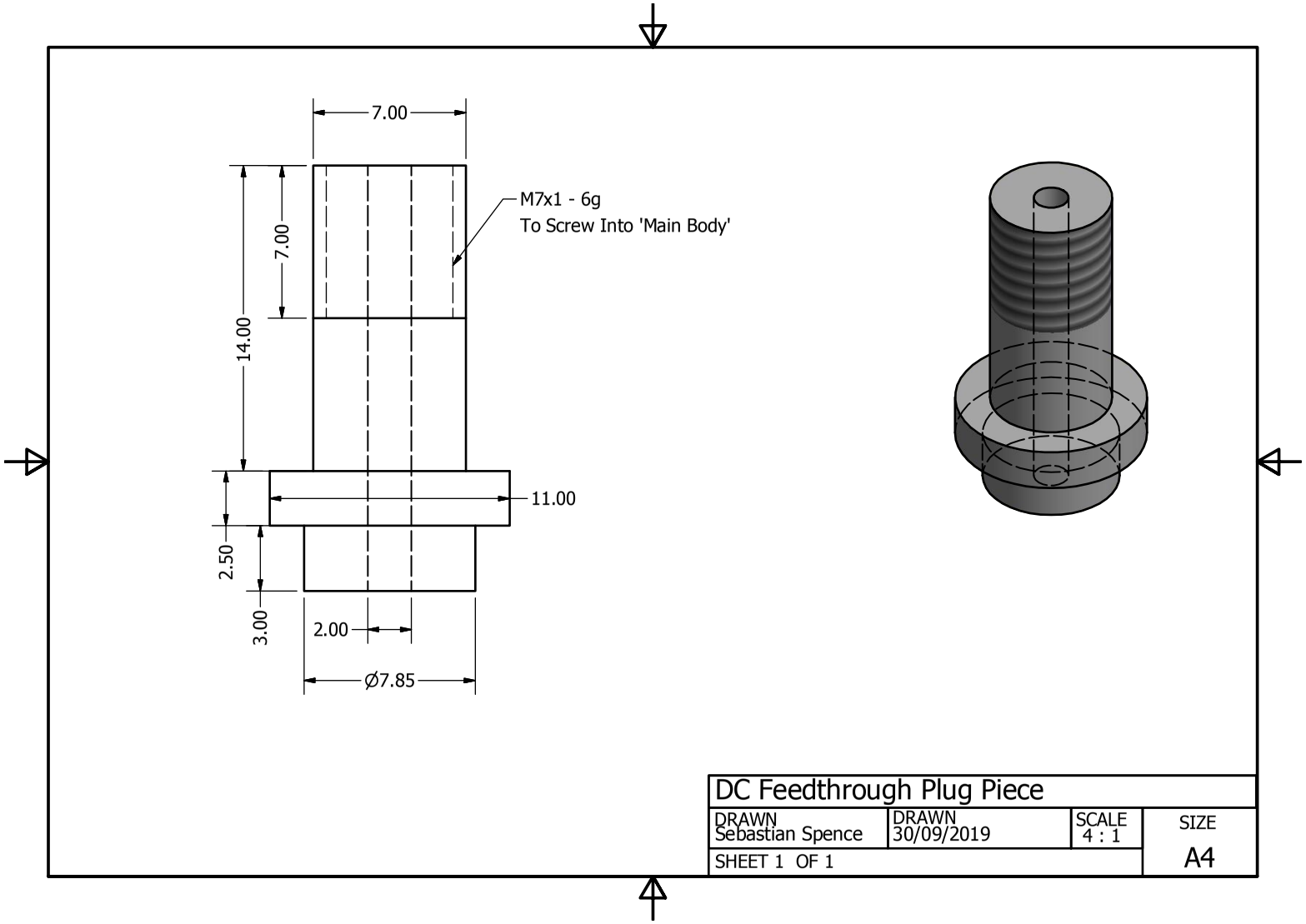

Figure 15: Plug piece for preamp feedthrough.

C 1K Pot Top Collar

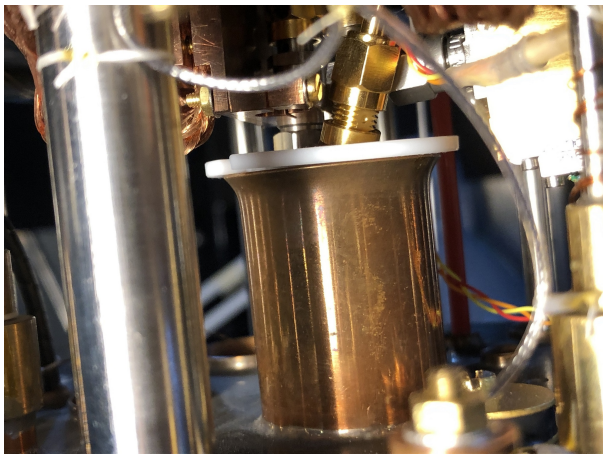

Figure 16: Photo showing top of 1K pot, showing space restriction and also central tube with white teflon collar.

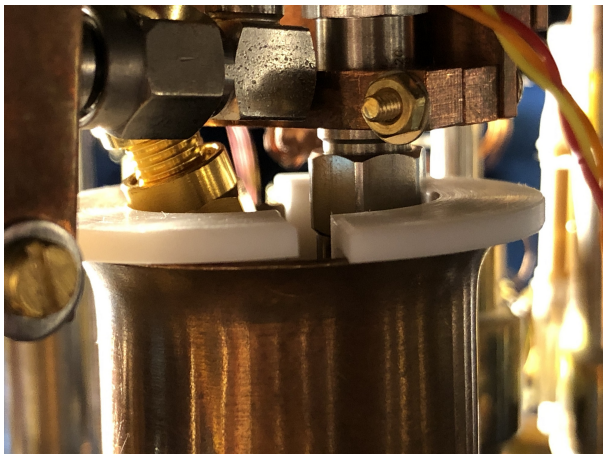

Figure 17: Close up photo of 1K pot central tube with white teflon collar. Also showing in and out coaxial microwave lines with SMA connectors.

D Square Cavity Pieces

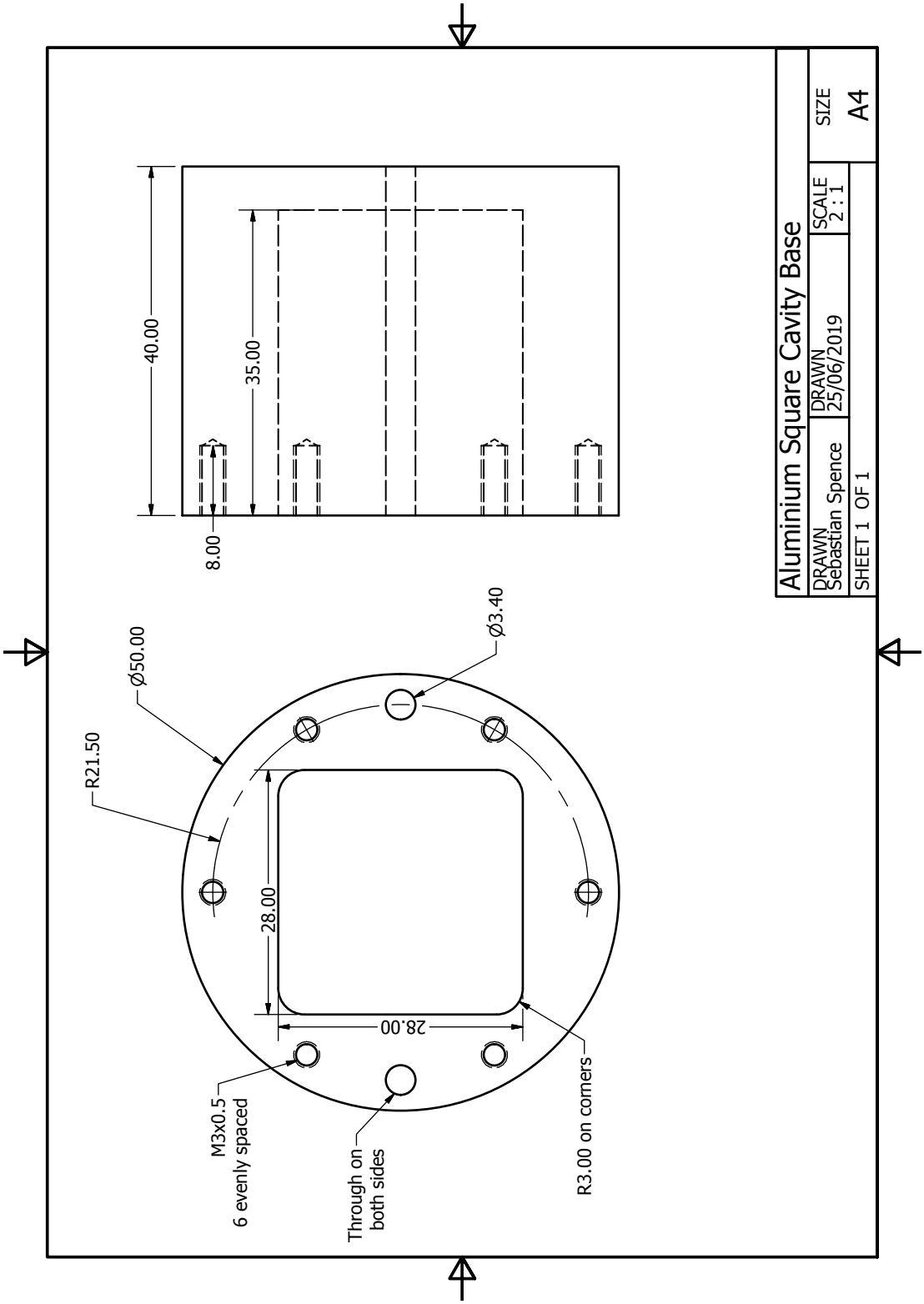

Figure 18: Base piece for square aluminium cavity.

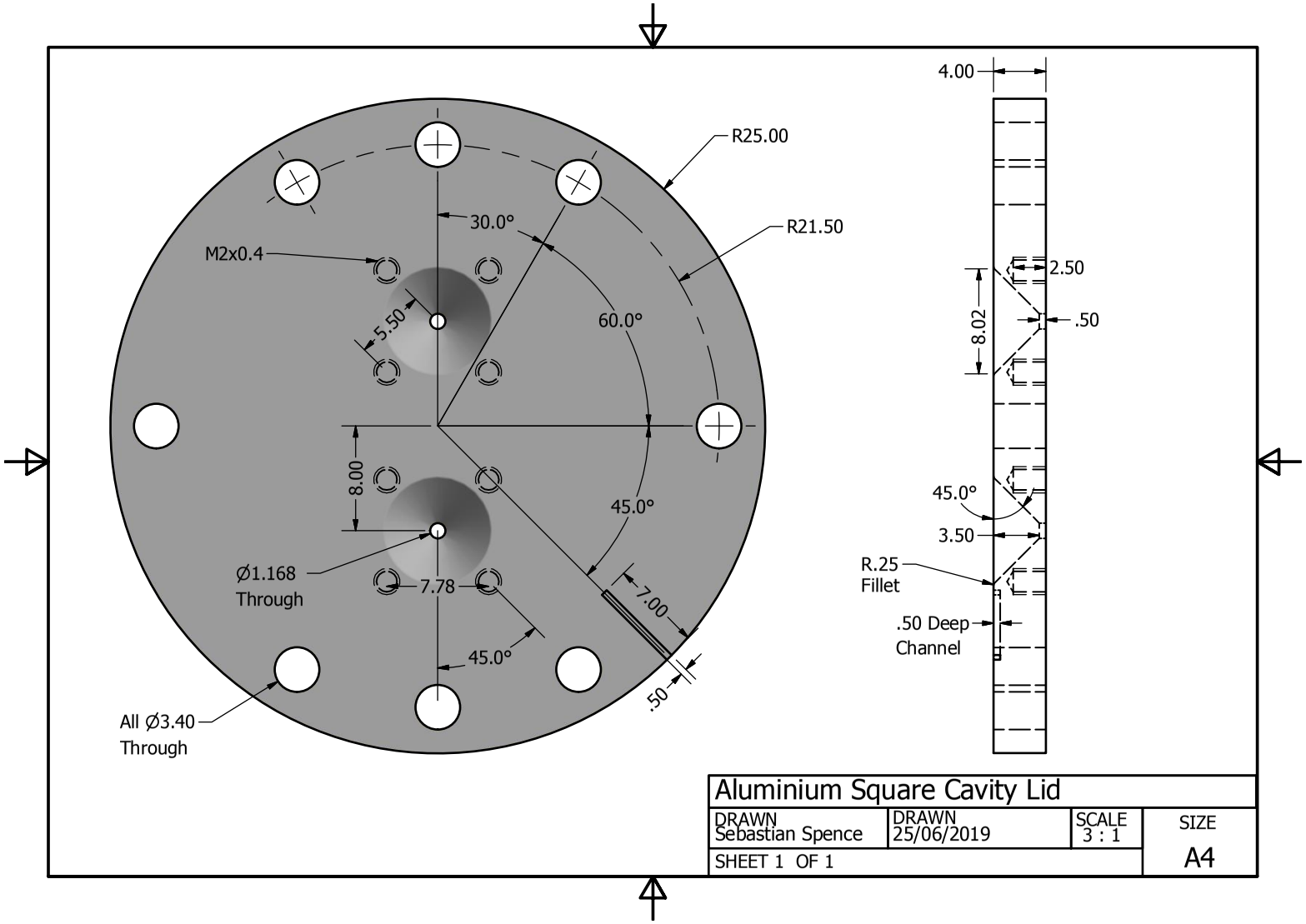

Figure 19: Lid piece for square aluminium cavity.

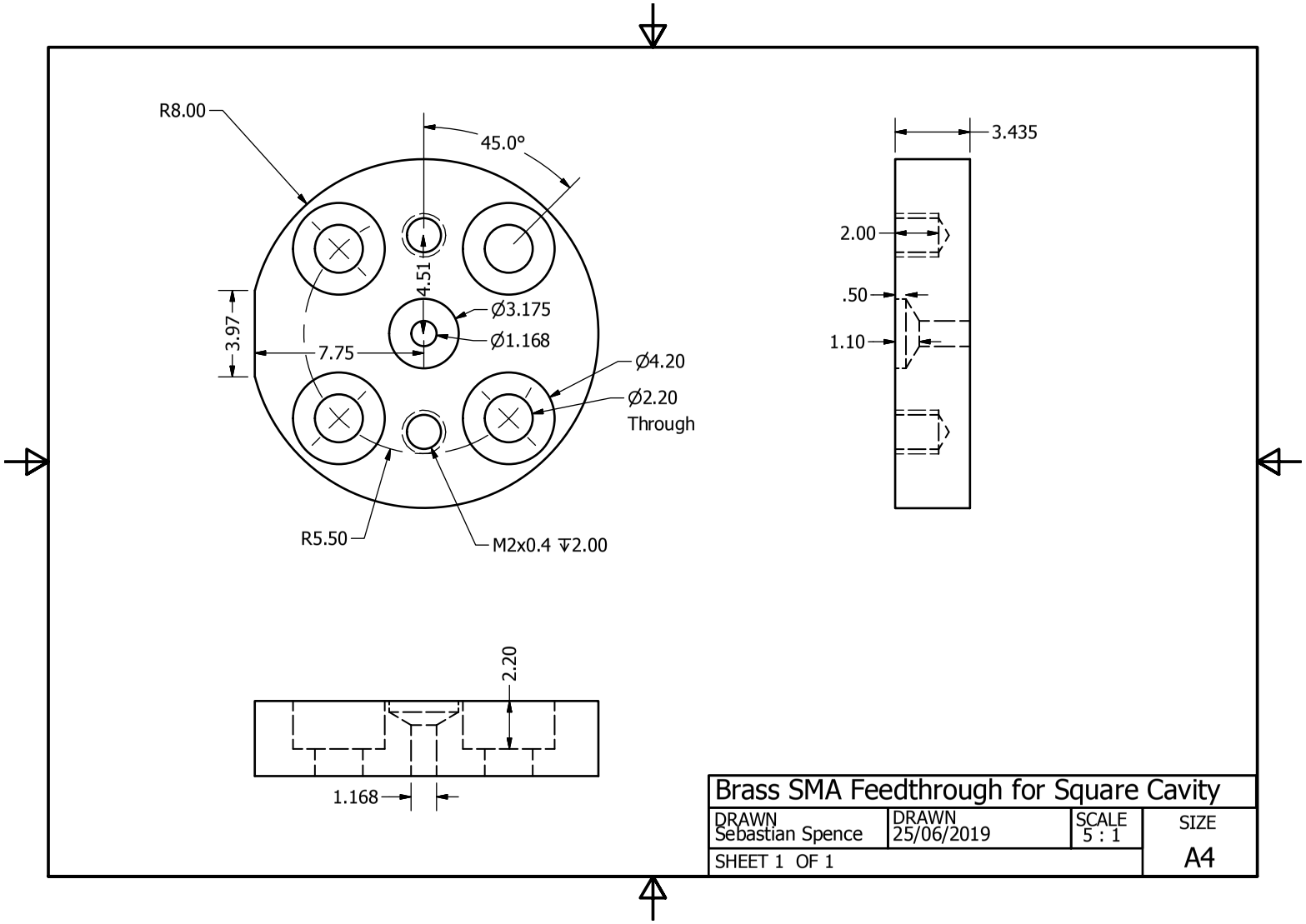

Figure 20: Brass SMA feedthrough piece for square aluminium cavity.

E Initial Re-entrant Cavity Pieces

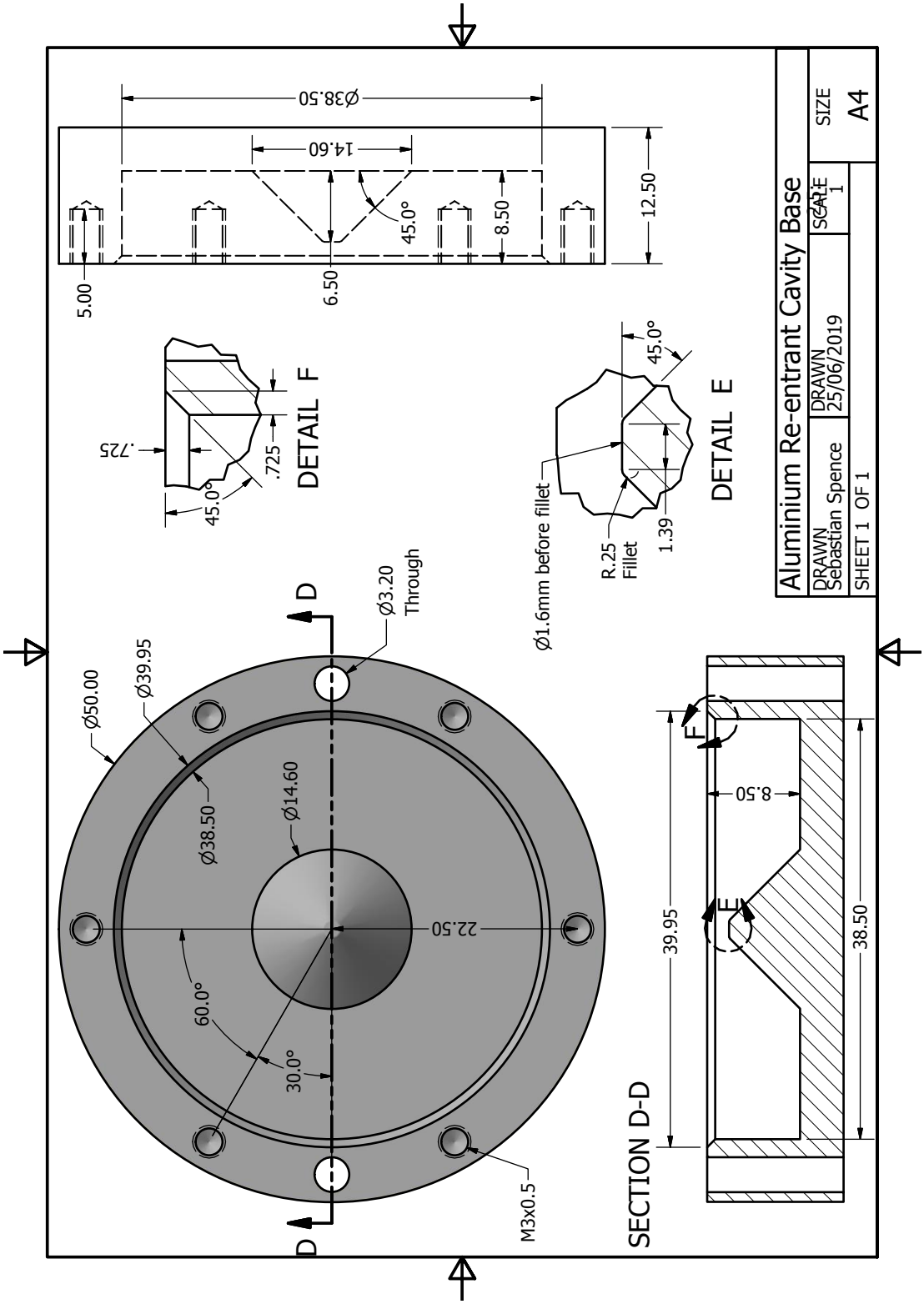

Figure 21: Base piece for re-entrant aluminium cavity.

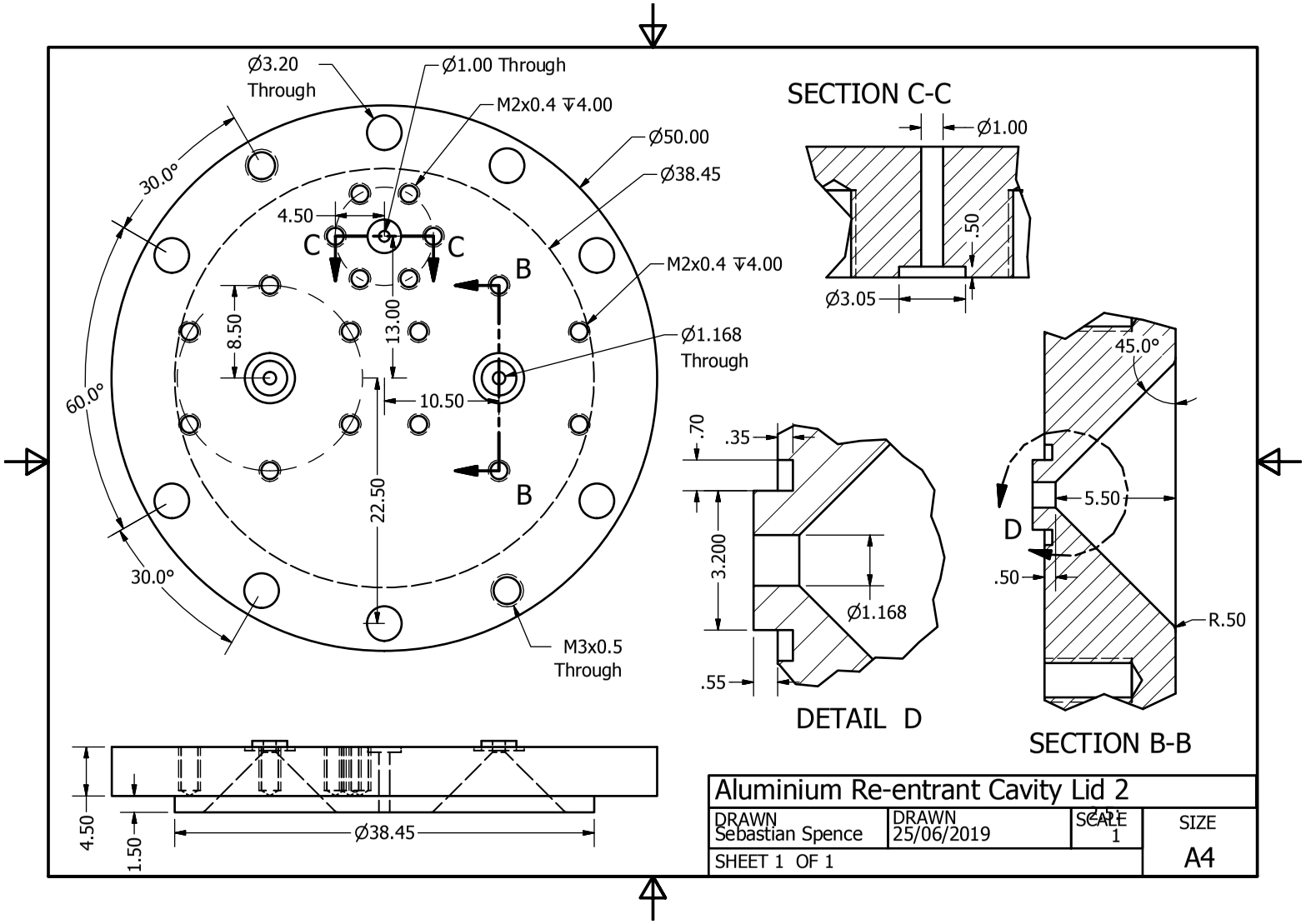

Figure 22: Lid piece for re-entrant aluminium cavity.

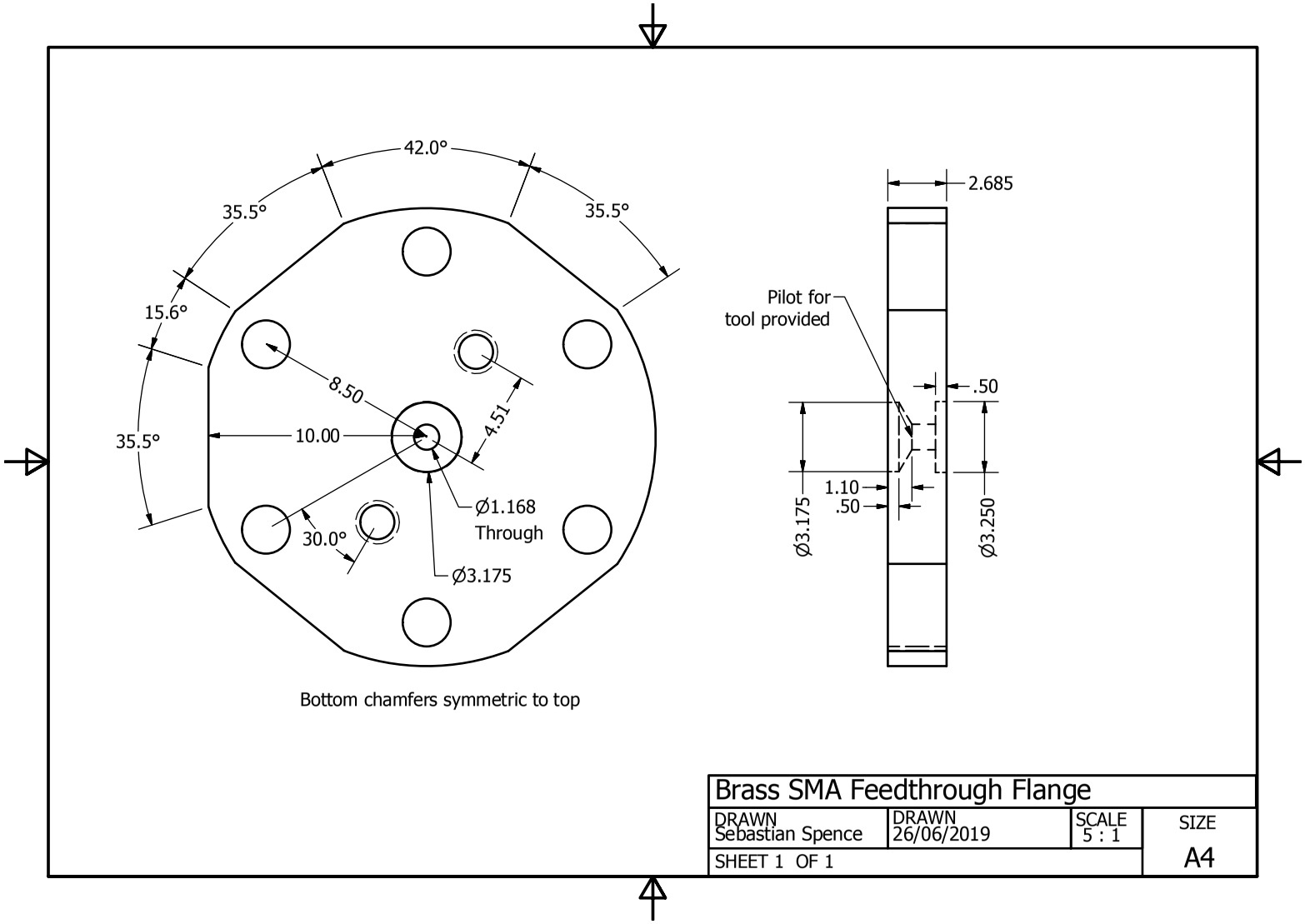

Figure 23: Brass SMA feedthrough piece for re-entrant aluminium cavity.

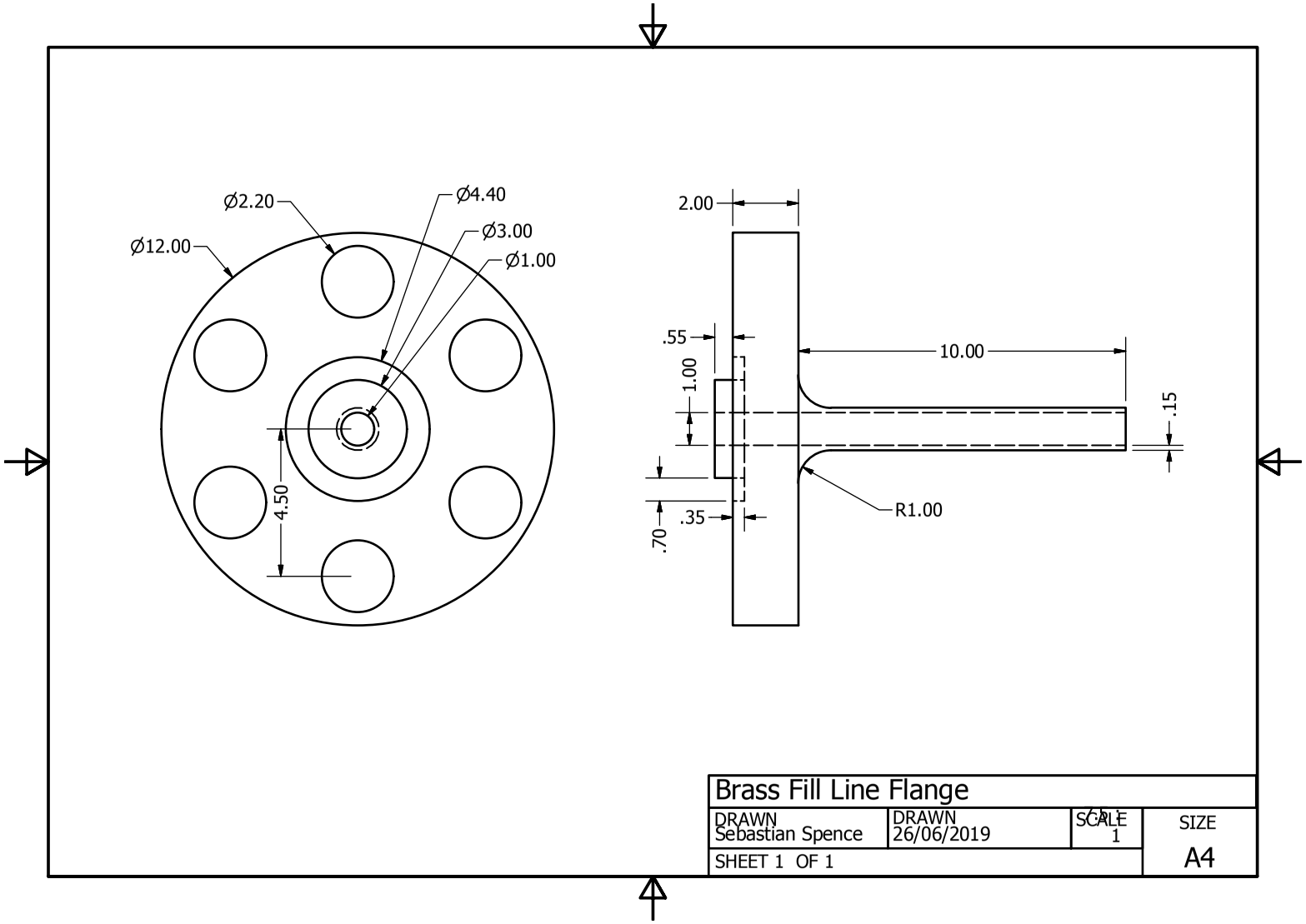

Figure 24: Brass Fill line piece for re-entrant aluminium cavity.

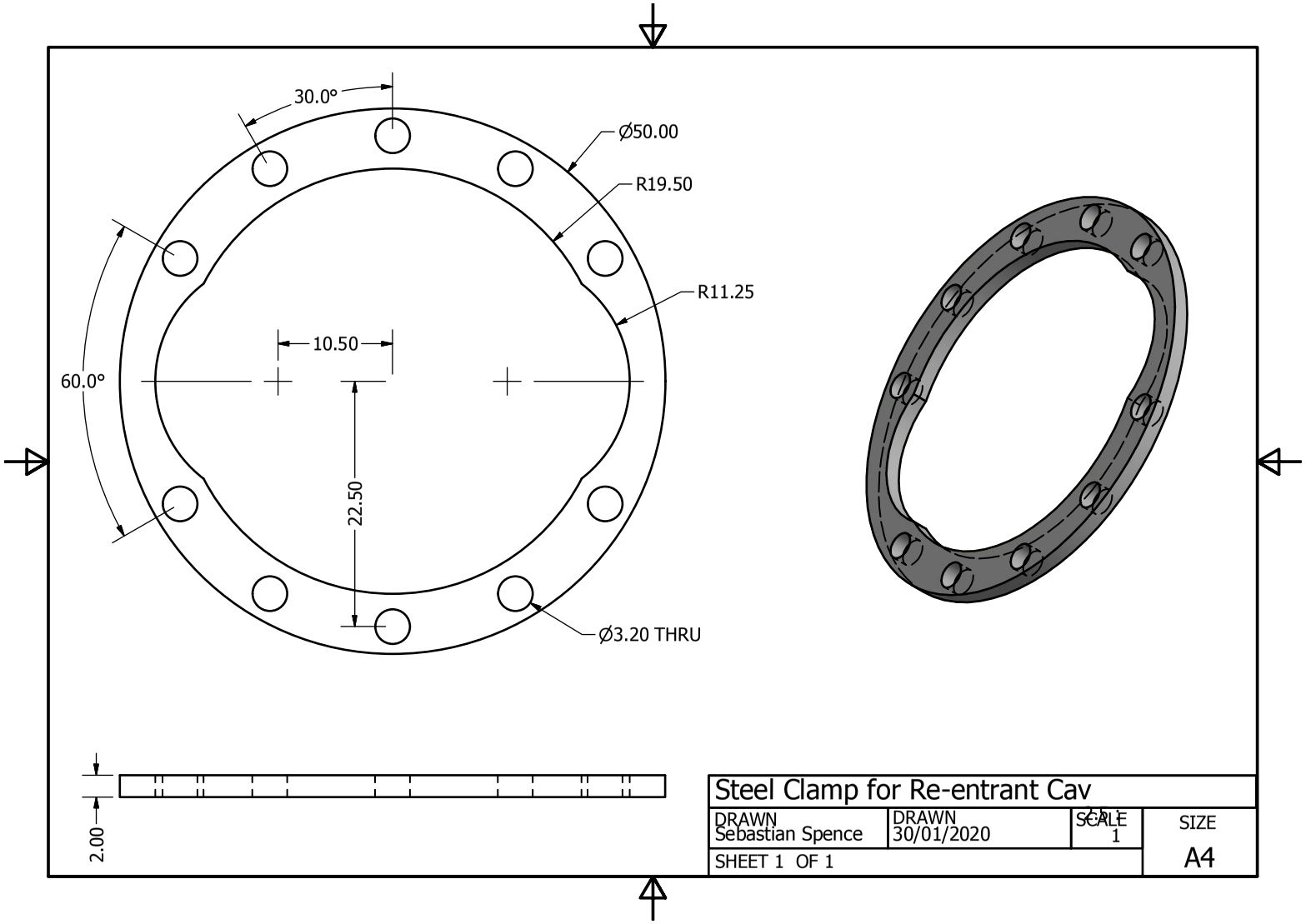

Figure 25: Stainless steel clamp piece for re-entrant aluminium cavity.

F Redesigned Re-entrant Cavity Pieces

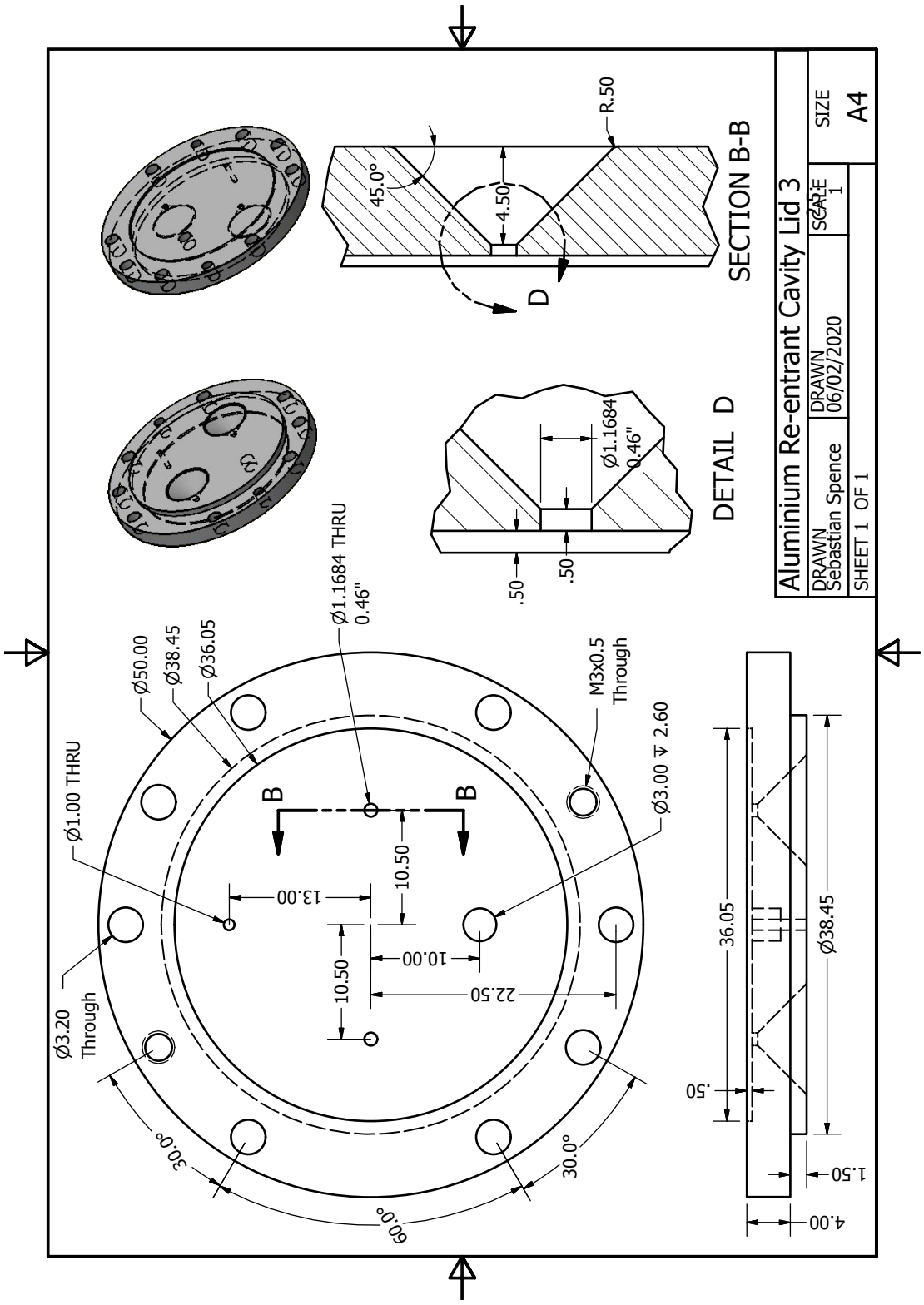

Figure 26: Redesigned lid piece for re-entrant aluminium cavity.

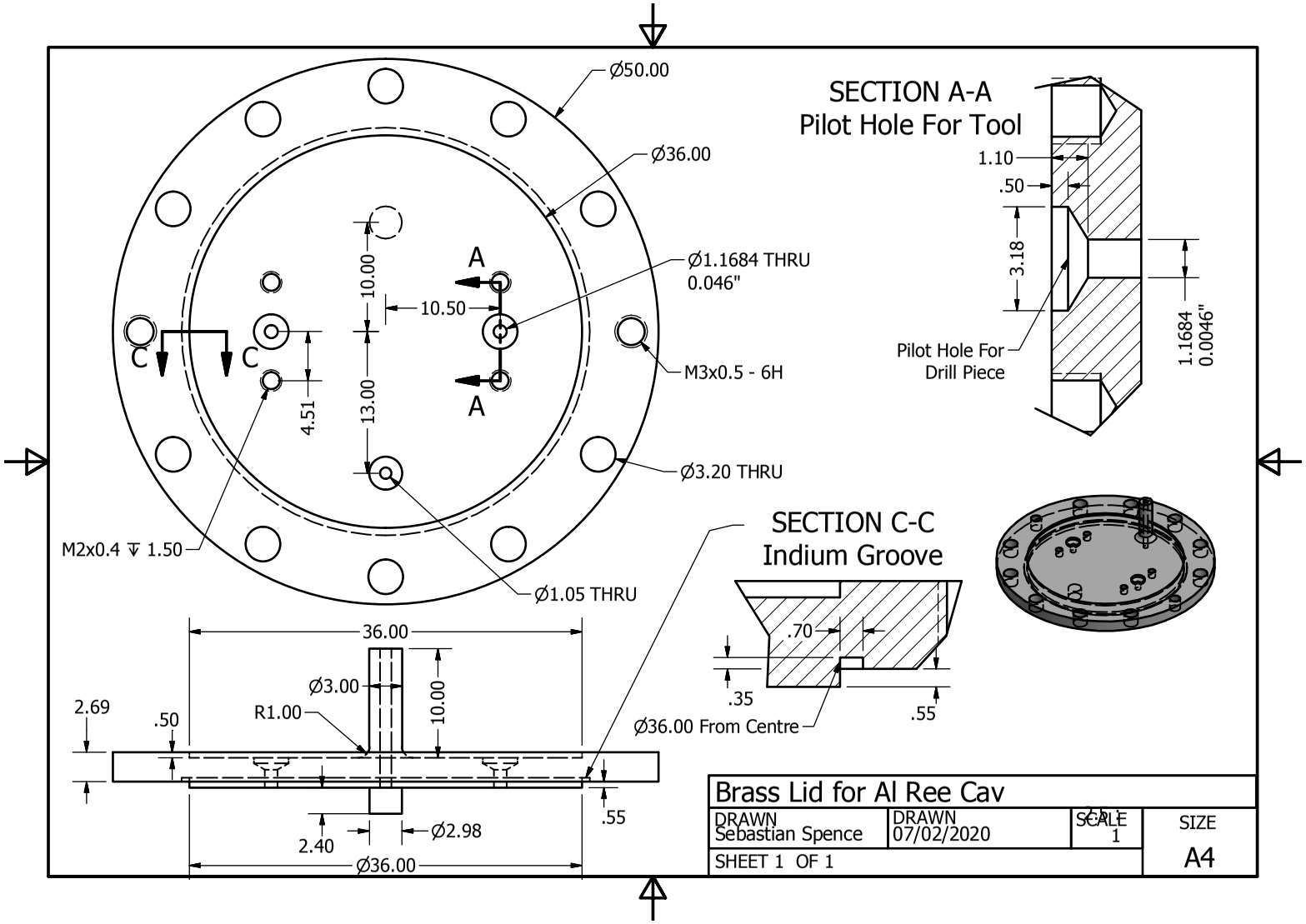

Figure 27: Brass top piece for re-entrant aluminium cavity, including both SMA feedthroughs and also fill line.

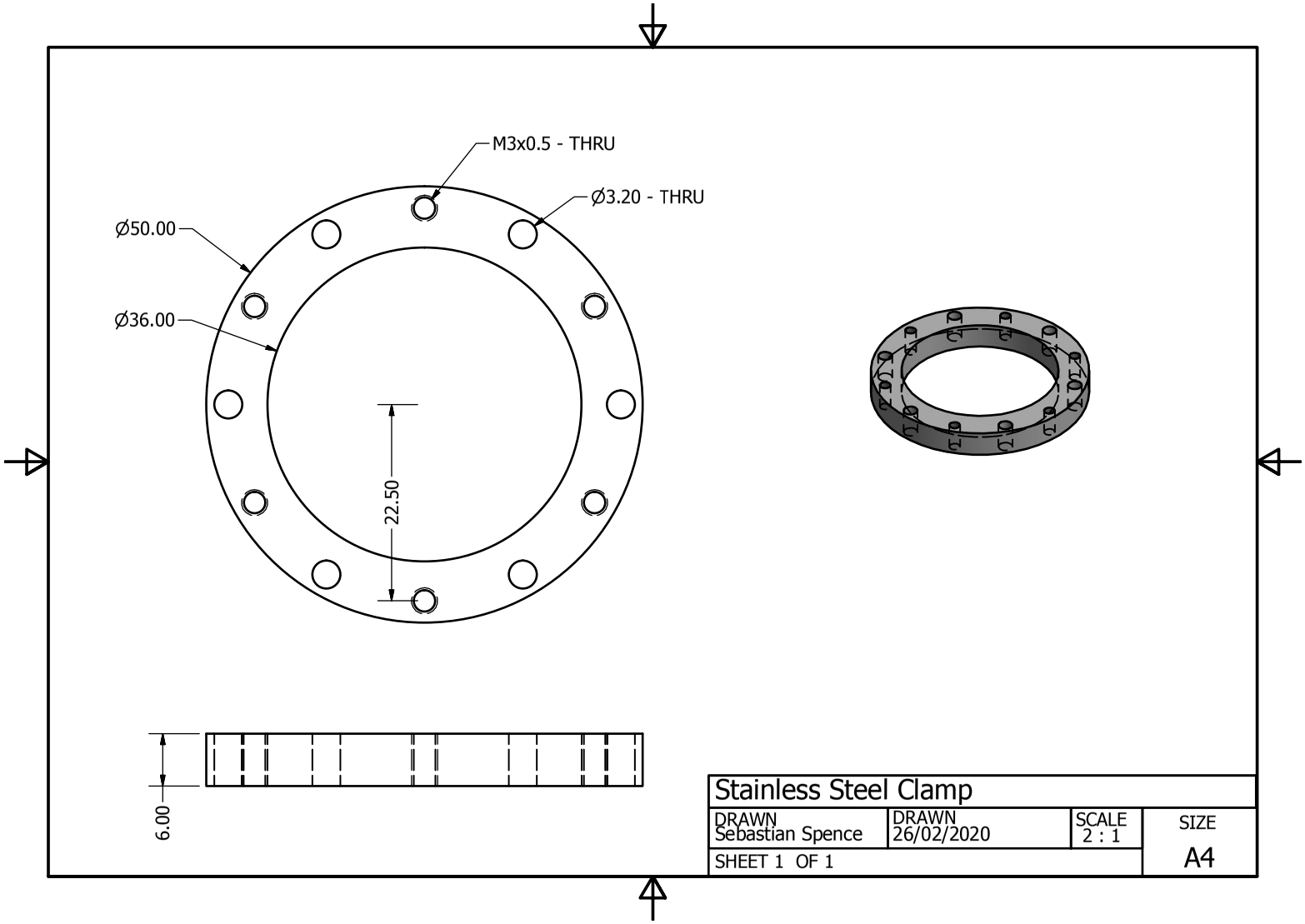

Figure 28: Second stainless steel clamp piece for re-entrant aluminium cavity.

G Hermetic Feedthrough Installation

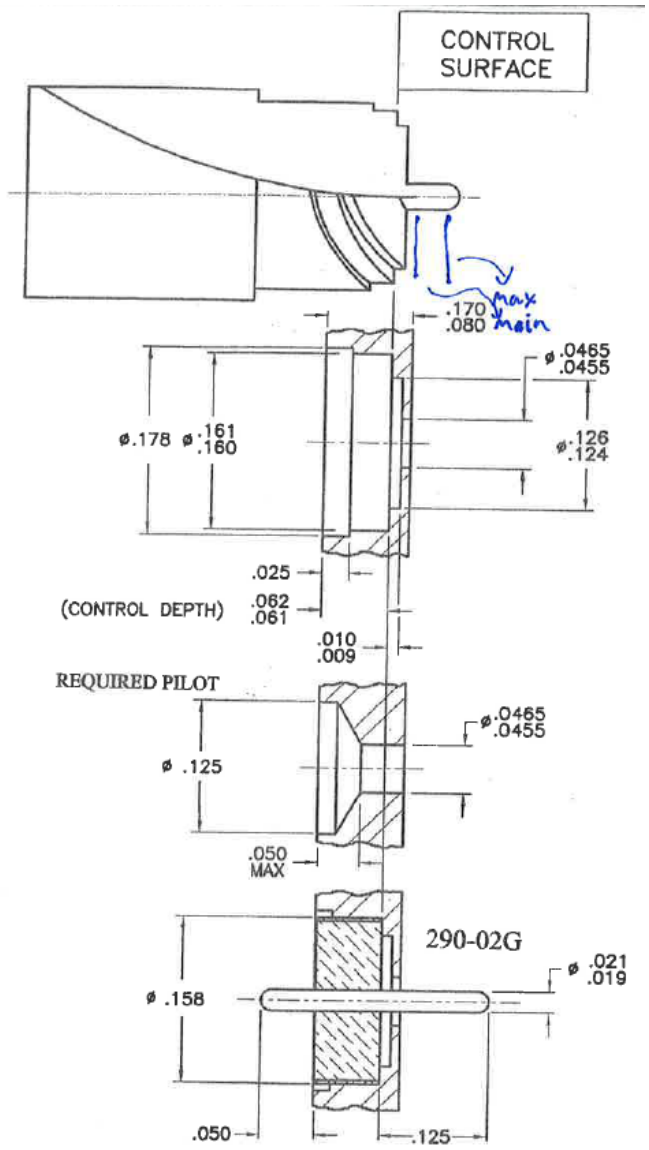

Figure 29: Section of technical document showing dimensions of drilled hole for feedthrough installation and of pilot hole required before drilling.

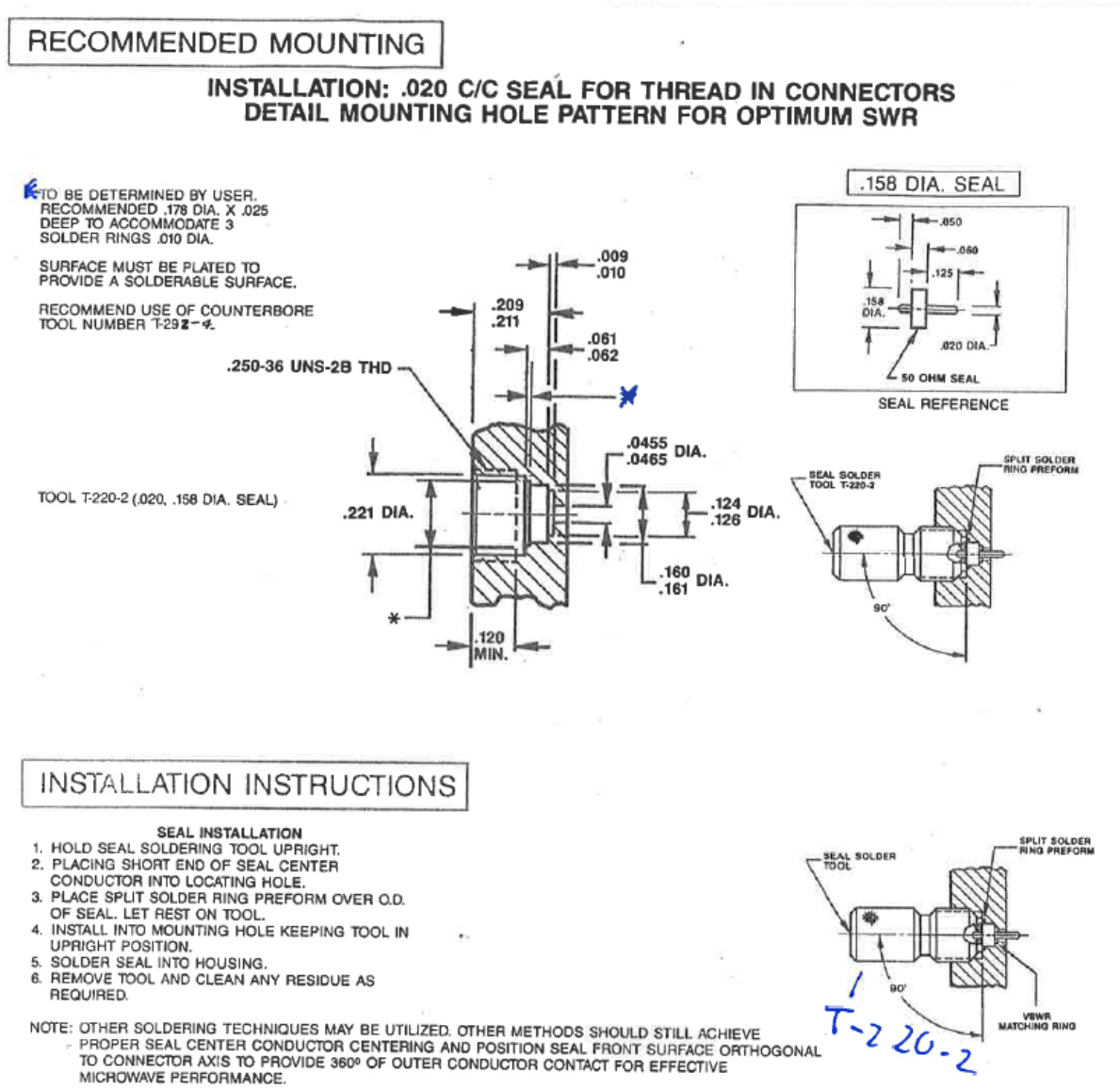

Figure 30: Section of technical document detailing the thread in installation of a hermetic feedthrough, this id not quite correct as we are not using the thread in SMA connectors, but has useful information for seal installation.